IDŐJÁRÁS

QUARTERLY JOURNAL
OF THE HUNGARIAN METEOROLOGICAL SERVICE

CONTENTS

VOL. 101 * NO. 1 * JANUARY–MARCH 1997

IDŐJÁRÁS

Quarterly Journal of the Hungarian Meteorological Service

Editorial Office: P.O. Box 39, H-1675 Budapest, Hungary or
Gilice tér 39, H-1181 Budapest, Hungary
E-mail: gmajor@met.hu or *antal@met.hu*
Fax: (36-1) 290-7387

Subscription by

mail: IDŐJÁRÁS, P.O. Box 39, H-1675 Budapest, Hungary;
E-mail: gmajor@met.hu or *antal@met.hu*; *Fax: (36-1) 290-7387*

IDŐJÁRÁS

Quarterly Journal of the Hungarian Meteorological Service
Vol. 101, No. 1, January–March 1997, pp. 1–15

A one-dimensional thermal numerical model of morning convective boundary layer development

R. Mitzeva, St. Evtimov and **S. Doychinska**

Department of Meteorology, Faculty of Physics, University of Sofia,
5, J. Bourchier, Sofia–1126, Bulgaria
E-mail: rumypm@phys.uni-sofia.bg

(Manuscript received 12 December 1995; in final form 13 November 1996)

Abstract—A one dimensional numerical model of the evolution of the morning *convective boundary layer* (CBL) is developed. The basic assumption is that heat in the CBL is transported mainly by discrete convective elements — thermals. A governing equation for the vertical profile of the horizontal-mean potential temperature is derived by partitioning the CBL at each level and at each moment in two domains, one covered with thermals and the other occupied by downdrafts. The problem is closed by assuming that the thermals evolve as individual ones interacting with the environmental air by buoyancy and entrainment mechanisms.

The model was tested for both simulated and measured initial temperature soundings. The calculations demonstrate a two-stage type formation of the CBL. During the first stage the potential temperature lapse rate gradually decreases and the temperature inversion erodes in a layer of growing thickness. The CBL is formed only in the second stage and it occupies at once the layer of the already destroyed inversion. After that only its height increases. The calculations with different magnitudes of the radiation heating indicate that the CBL formation is possible only if that magnitude exceeds a critical value. Sensitivity studies were performed for two types of size distribution of thermals at the earth's surface.

Key-words: convective boundary layer, thermals, numerical model, nocturnal ground temperature inversion.

1. Introduction

Analyzing his own atmospheric measurements of the *convective boundary layer* (CBL) *Telford* (1992) concluded that convective transport is a process where isolated thermal elements carry practically all the quantities such as heat and moisture from one level to another. Observational studies of *Lenschow* and *Stephens* (1982), *Young* (1988) and *Hunt et al.* (1988) clearly indicate a 'thermal-like' structure of the CBL. According to these measurements thermals

are buoyancy-driven convective eddies which generate most of the turbulence in the unstable atmospheric boundary layer. The CBL is composed of thermal updrafts and their compensating environmental downdraft. A number of numerical models of the CBL development (*Telford*, 1966; *Manton,* 1975; *Andreev* and *Ganev,* 1981; *Roisin,* 1982; *Chatfield* and *Brost* 1987) realized these concepts.

This paper presents a one-dimensional numerical model of the morning CBL evolution due to the heat transfer by thermals. The thermals originate near the earth's surface during the morning hours when the ground is strongly heated by the solar radiation. Therefore, the model describes the penetrative convection in presence of a time-dependent heating forcing. In this case the turbulence is buoyancy-driven and the model is valid in the case of strong insolation and absence of wind and clouds.

The theoretical background and the derivation of the governing equations of the model are given in Section 2. The numerical scheme is presented in Section 3. The results of the numerical simulations with the model are given in Section 4. They are discussed in the final section of the paper.

2. Model description

The basic idea of the model is that heat in the CBL is transfered by discrete convective elements (buoyant parcels or thermals) and compensating environmental downdrafts. It means that at the parametrization of the CBL with respect to the velocity field the CBL has to be separated into updrafts or thermals, which are convective elements originating near the surface, and downdrafts — a domain outside the updrafts with a compensating mean downward velocity. Similar separation is used for example in *Andreev* and *Ganev* (1981), *Roisin* (1982), *Chatfield* and *Brost* (1987).

The observations show that the updrafts have more velocity fluctuations while the downdraft velocity distribution is rather narrow and it has a mode approximately equal to the average downdraft velocity (*Lamb*, 1982). Thus, representing the downdraft velocity by a mean velocity which is a function of height and time should be a rather good approximation, while for the vertical velocity it is better to use thermals with various sizes. This separation should also be valid for the other CBL characteristics, because the velocity controls their spatial and temporal distributions. Thus, a horizontal area of the CBL $S(z,t)$ at a given level and at a given moment can be partitioned in two domains — the first one with area $S_T(z,t)$ covered with thermals and the second one with area $S_e(z,t)$ occupied by downdrafts of environmental air (see *Fig. 1*). Obviously the horizontal-mean value $\bar{A}(z,t)$

$$\overline{A}(z,t) = \frac{1}{S}\int_{S} A(x,y,z,t)\,dx\,dy \tag{1}$$

of some CBL characteristic may be separated as

$$\overline{A} = \overline{A}_T + \overline{A}_e, \tag{2}$$

where

$$\overline{A}_T = \frac{1}{S}\int_{S_T} A\,dx\,dy \quad \text{and} \quad \overline{A}_e = \frac{1}{S}\int_{S_e} A\,dx\,dy. \tag{3}$$

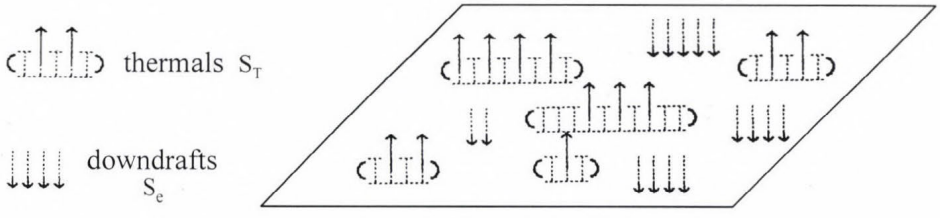

Fig. 1. Schematic illustration of the partition of CBL at a given level at a given time into thermals (updrafts) and downdrafts domains.

It has already been mentioned that the horizontal fluctuations of the downdraft characteristics are small. Therefore, approximately

$$\overline{A}_e = \frac{S_e}{S}A^*, \tag{4}$$

where A^* is a value of A in the environmental air, which is assumed to be horizontally uniform.

Following Eqs. (4) and (2) A^* may be expressed as

$$A^* = \frac{S}{S_e}\left(\overline{A} - \overline{A}_T\right). \tag{5}$$

It is supposed that the air is dry. Then after the application of the averaging given by Eq. (1) the continuity and heat equations for the atmospheric boundary layer become (*Matveev*, 1981) :

$$\frac{\partial}{\partial z}\,\overline{w} = 0, \tag{6}$$

$$\frac{\partial}{\partial t}\,\overline{\theta} = -\frac{\partial}{\partial z}\,\overline{w\theta}. \tag{7}$$

In Eq. (6) and Eq. (7) $\overline{w}$, $\overline{\theta}$ and $\overline{w\theta}$ are the horizontal-mean vertical velocity, potential temperature and vertical convective heat flux, respectively.

From Eq. (6) it follows that $\overline{w} = 0$, because at flat earth's surface the horizontal-mean vertical velocity vanishes. Eq. (5) gives

$$w^* = -\frac{S}{S_e}\,\overline{w}_T \quad \text{and} \quad \theta^* = \frac{S}{S_e}\left(\overline{\theta} - \overline{\theta}_T\right).$$

Now it can easily be obtained that

$$\overline{w\theta} = \left(\overline{w\theta}\right)_T - \frac{S}{S - S_T}\,\overline{w}_T\left(\overline{\theta} - \overline{\theta}_T\right),$$

and the heat Eq. (7) takes the final form

$$\frac{\partial}{\partial t}\,\overline{\theta} = -\frac{\partial}{\partial z}\left[\left(\overline{w\theta}\right)_T - \frac{S}{S - S_T}\,\overline{w}_T\left(\overline{\theta} - \overline{\theta}_T\right)\right]. \tag{8}$$

Let $f(R,z,t)$ be the number of thermals with radius R per unit area at level z and at time t. The fraction of the area occupied by rising thermals at fixed level and time is

$$\frac{S_T}{S} = \sum_R \pi R^2 f(R,z,t), \tag{9}$$

where the sum is over all thermals' radii.

Following Eq. (3) one can get for the updraft characteristics of the CBL

$$\overline{\theta}_T = \sum_R \pi R^2\,\theta\,(R,z,t) f(R,z,t),$$

$$\left(\overline{w\theta}\right)_T = \sum_R \pi R^2 W(R,z,t)\,\theta\,(R,z,t) f(R,z,t), \tag{10}$$

$$\overline{w}_T = \sum_R \pi R^2 W(R,z,t) f(R,z,t),$$

where $W(R,z,t)$ and $\theta(R,z,t)$ are the vertical velocity and the potential temperature of the rising thermals with radii R which are at level z at moment t.

Substituting Eq. (10) in Eq. (8) yields

$$\frac{\partial}{\partial t}\overline{\theta} + \frac{\partial}{\partial z}\left[B(z,t)\overline{\theta}\right] = C(z,t), \tag{11}$$

where

$$B(z,t) = -\frac{1}{1-(S_T/S)}\sum_R \pi R^2 Wf, \tag{11a}$$

$$C(z,t) = -\frac{\partial}{\partial z}\left[\frac{1}{1-(S_T/S)}\left(\sum_R \pi R^2 Wf\right)\left(\sum_R \pi R^2 \theta f\right) + \sum_R \pi R^2 W\theta f\right] \tag{11b}$$

and S_T/S is given by Eq. (9).

The temperature at the earth's surface follows the changes of the solar radiation and the lower boundary condition in the model is

$$\overline{\theta}(0,t) = \overline{\theta}_0(0) + k\sin(2\pi t/24), \tag{12}$$

where $\bar{\theta}_0(0)$ is the potential temperature at the earth's surface at the moment of sunrise, and k gives the increase of the earth's surface temperature in 6 hours. The parameters k and $\bar{\theta}_0(0)$ in Eq. (12) are varied in the numerical experiments.

At the limit of large z the initial potential temperature profile $\bar{\theta}_0(z)$ is unperturbed since the CBL has a finite depth during its evolution. Hence, the initial and upper boundary conditions in the problem are respectively:

$$\overline{\theta}(z,0) = \overline{\theta}_0(z), \quad \overline{\theta}(z,t) \to \overline{\theta}_0(z),$$

at large z.

The terms $B(z,t)$ and $C(z,t)$ in Eqs. (11a) and (11b) are unknown. They depend on the individual characteristics of the rising thermals with different radii and on the size statistics of the thermals. Therefore the problem is to evaluate the thermals' characteristics and their size distribution. Some additional

assumptions are needed for that purpose. The CBL is a composition of thermals and environmental air. The interaction between each thermal and the surrounding air is realized by the entrainment mechanism and the buoyancy effect due to the temperature excess. In the present model following *Andreev* and *Ganev* (1981) it is assumed that the thermals are spheres with radii R_i, vertical velocities W_i and potential temperatures θ_i and that they ascend as individual thermals. The time evolution of W_i and θ_i during the thermal's rising are given by (*see Andreev* and *Panchev*, 1975)

$$\frac{d}{dt}W_i = -\alpha W_i^2 + g\left[\frac{\theta_i - \bar{\theta}}{\bar{\theta}}\right], \tag{14}$$

$$\frac{d}{dt}\theta_i = -\alpha\left(\theta_i - \bar{\theta}\right)W_i, \tag{15}$$

and

$$\frac{d}{dt}z_i = W_i,$$

where g is the acceleration due to gravity and z_i is the coordinate of thermal's mass center, $R_i = R_{i0} + 0.2z_i$, R_{i0} is the thermal's radius near the earth's surface. The entrainment parameter α is

$$\alpha(z_i, R_i) = \frac{0.6}{R_i(z_i)}.$$

Some information on the thermal size distribution $f(R,z,t)$ is necessary for the closure of the problem. In the model $f(R,z,t)$ is numerically evaluated in the manner described in the next section.

3. Numerical scheme

Eq. (11) together with the initial and boundary conditions (Eqs. (12) and (13)) is solved numerically using an explicit finite-difference scheme.

It has been already mentioned that the problem is to evaluate the terms $B(z,t)$ and $C(z,t)$ in Eqs. (11a, 11b). The calculation of the sums in Eqs. (11a, 11b) requires some information about the characteristics of the rising thermals

and their size distribution at any level and at any moment. Numerical solutions of Eq. (14) to Eq. (16) for thermals with various initial radii R_{i0} provide the necessary information about W_i, θ_i and z_i at any time step. For the determination of the distribution function $f(R,z,t)$ the spherical thermals are transformed into cylinders with the same radius R_i and volume as the sphere. Thus the heights of the cylinders will be given by

$$H_i = \frac{3}{4} R_i. \tag{17}$$

It is supposed that at a given moment the thermal with radius R_i located at height z_i affects the levels between z_i and $z_i - H_i$. Hence the distribution function $f(R,z,t)$ for a given level z at a given moment t is the sum of the thermals with radii R_i affecting the level z. Obviously $f(R,z,t)$ depends on the size distribution of thermals at the earth's surface.

The level $z = 0$ in the model was set to be the level of the thermals starting.

The initial potential temperature profile $\bar{\theta}(z,0)$ is interpolated to determine the potential temperature at the vertical grid levels.

The evolution of potential temperature profiles for a time step is obtained as follows:

- The Eqs. (14) to (16) are numerically integrated by the Runge-Kutta method using $\bar{\theta}(z,t)$. Thus W_i, θ_i and z_i are calculated for a time step.
- The discrete size distribution function $f(R,z,t)$ is determined as the sum of the thermals with radii R_i which at a given moment t affect the levels z situated between z_i and $z_i - H_i$.
- The terms $B(z,t)$ and $C(z,t)$ are calculated from Eqs. (11a, 11b) and $\bar{\theta}(z,t + dt)$ is obtained from Eq. (11) by an explicit finite-difference scheme. For the levels not affected by the rising thermals at a given moment t, $f(R,z,t) = 0$ and $\bar{\theta}(z,t + dt) = \bar{\theta}(z,t)$.

These calculations are repeated until all the thermals reach the levels at which their velocities $W_i = 0$. In the model it is accepted that a new thermal group with a given distribution function starts at the earth's surface when the previous group stops, but not more often than every 15 minutes.

The calculations have been carried out using a time step $dt = 1s$ and a vertical grid length $dz = 50$ m. For the stabilization of the numerical scheme the potential temperature at each grid level z is recalculated as

$$\bar{\theta}(z,t) = \frac{1}{2}\left(\bar{\theta}(z + dz) + \bar{\theta}(z - dz)\right).$$

4. Numerical simulations and results

The purpose of the numerical simulations was to study the general behavior of the model, as well as its response to variation of the control parameters.

The model requires an initial sounding and initial size distribution, vertical velocities and temperature excesses of thermals at the earth's surface to be preassigned. Their values were chosen to be of the same order of magnitude as in the observations.

The measurements of *Warner* and *Telford* (1967) showed that thermals were typically 200–300 m in horizontal extent with an initial upward velocity of about 1 m/s and a temperature excess of about 1 K. The observations of *Vulfson* (1961) showed that the average size of the convective elements was 50–100 m. Various experimental estimates of the fraction of area covered with thermals are reported in the literature. *Warner* and *Telford* (1967) and *Frish* and *Businger* (1973) gave a value of 0.4, while *Lenschow* and *Stephens* (1980) recommended 0.25. *Young's* (1988) measurements showed that the fraction of area covered with thermals decreased with height up to the half of the CBL and then increased with height.

For all model simulations the starting velocities of the thermals were fixed to be 1 m/s and the temperature excess was set to be 1 K. Two types of size distribution (the number of thermals with a given diameter per km^2) at the earth's surface were used. The first type which will further be denoted as ST1 is presented in *Table 1*. *Andreev* and *Ganev* (1981) extracted that distribution from *Vulfson's* (1961) data. The second type of size distribution, ST2 is uniform — during the first six hours after sunrise there are 0.5 thermals per km^2 with diameters from 50 m to 250 m at intervals of 50 m. While ST1 is in accordance with some observations, ST2 is more or less speculative in order to test the sensitivity of the model to the type of the thermals' size distribution. In both cases the fraction of area covered with thermals was fixed to be 0.22 at the earth's surface. Four different values for $k(k = 5,6,7,8)$ were used in Eq. (12) to study the response of the model to the magnitude of the surface heating. These values allow to model adequately the real spring diurnal temperature variations in Sofia, Bulgaria.

The sensitivity to the initial sounding was tested by running the model from two initial temperature profiles, which were model inversions with constant lapse rates. They are given with solid lines on *Fig. 2* and *Fig. 3*. Being nocturnal ground inversions, the layers between 0 and 600 m had lapse rates $\gamma = -0.5$ K/100 m and $\gamma = -1$ K/100 m, respectively. The initial temperature profiles above 600 m were identical in both cases and they had temperature lapse rates of 0.5 K/100 m. The calculations were carried out at $k = 7$. The initial thermal size distribution was of type ST1.

Fig. 2 and Fig. 3 show that according to the model calculations the heat transfer by rising thermals and compensating downdrafts causes temperature

profile changes in the direction of decreasing air stability during the first hours. The CBL is not fully developed three hours after sunrise in both simulations, but the temperature inversion is eroded up to 350 m for the case with γ = –0.5 K/100 m (Fig. 2) and up to 250 m for the case with γ = –1 K/100 m (Fig. 3). The results show that the lapse rate of horizontal-mean potential temperature decreases gradually with the increase of solar radiation. Four hours after sunrise it is zero up to 400 m for the case with γ = –0.5 K/100 m (Fig. 2), i.e. at that moment the CBL is developed up to 400 m. For this case the CBL height increases up to 450 and 500 m five and six hours after sunrise, respectively (Fig. 2). For the case with stronger inversion (γ = –1 K/100 m) five hours after sunrise the CBL height is about 100 m lower compared to the case with γ = –0.5 K/100 m (see Fig. *2* and Fig. 3).

Table 1. The size distribution of the thermals at the earth surface named ST1 in the text. The statistics is extracted from *Vulfson's* (1961) data by *Andreev* and *Ganev* (1981).

Diameter of the thermals (m)	Number of the thermals per km^2	
	Hours after sunrise 0–3	Hours after sunrise 3–6
5	0.6	1.4
15	4.5	11.2
25	4.9	14.0
35	6.2	14.8
45	6.4	15.5
55	6.2	15.5
65	6.1	14.8
75	4.9	13.5
85	5.7	12.1
95	5.1	10.1
105	4.5	7.7
128	2.3	1.7

Further numerical simulations were carried out using a real temperature sounding observed on 4 May 1988 during the Sofia experiment (see *Brunzov et al.*, 1992). This sounding was selected because the wind had been weak (less than 3 m/s) and there had been no advection and clouds on that day. The initial potential temperature profile calculated from the data of *Brunzov et al.* (1992) is given as a solid line on *Fig. 4*. It can be seen that after sunrise there is a ground temperature inversion up to 250 m and a temperature isotherm between 250 m and 400 m.

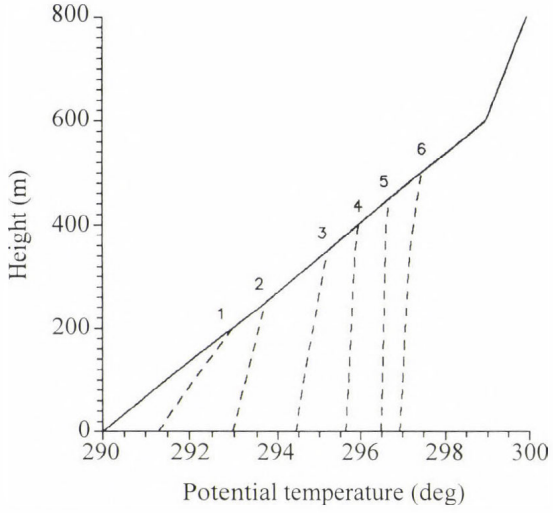

Fig. 2. Hourly vertical profiles of horizontal mean potential temperature (dashed lines). The numbers indicate hours after sunrise. The initial profile (solid line) represents temperature inversion with lapse rates γ = -0.5 K/100 m under 600 m and γ = -0.5 K/100 m above. The thermals have initial velocities 1 m/s, potential temperature excesses — 1 K and size distribution is of type ST1 (Table 1). The magnitude of radiation heating corresponds to k = 7.

The calculations show that if the parameter k is fixed to be k = 7, so that the surface temperature increases at a rate of 7 K/6 hours, and the initial thermal size distribution is of type ST1, there is no temperature inversion three hours after sunrise — the potential temperature lapse rate is 0.2 K/100 m up to 300 m. The CBL is fully developed four hours after sunrise up to 400 m and it rises with time up to 600 m six hours after sunrise (see Fig. 4). The measurements of *Brunzov et al.* (1992) indicate that the inversion is destroyed four hours after sunrise.

To test the response to the magnitude of solar heating the model was run with k = 5 (temperature increases at a rate of 5 K/6 hours), while the other parameters were unchanged. The calculation shows that in this case three hours after sunrise the temperature inversion is eroded up to 200 m, (potential temperature lapse rate is 0.33 K/100 m). As it is seen on *Fig. 5* the stability decreases gradually again, but the CBL is not developed even six hours after the beginning of the earth's heating.

The influence of the magnitude of radiation heating on the CBL development is clearly demonstrated on *Fig. 6a* and *Fig. 6b*. The potential temperature profiles four hours after sunrise are given on Fig. 6a. The same is plotted on Fig. 6b, but six hours after sunrise. The initial potential temperature profiles are plotted with solid lines. The parameter k, which controls the magnitude of radiation heating takes the values k = 5,6,7,8. The corresponding potential temperature profiles are plotted with asterisks and dashed lines with different sizes. The initial size distribution is of type ST1.

The results show that the stronger the heating is, the higher the convective boundary layer is developed. Obviously there is some threshold for the CBL development because while at $k = 5$ and $k = 6$ it is not developed at all, in the cases of $k = 7$ and $k = 8$ there are well developed convective mixed layers.

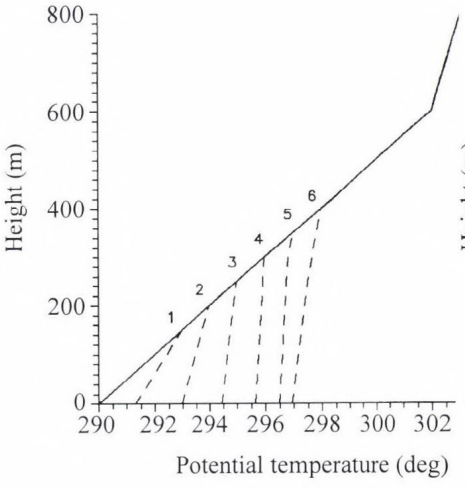

Fig. 3. As in Fig. 2 but for $\gamma = -1$ K/100 m.

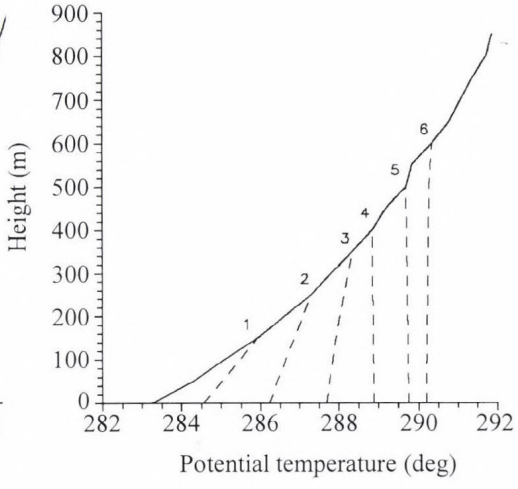

Fig. 4. As in Fig. 2 but the initial potential temperature profile is from real sounding (see *Brunzov et al.*, 1992).

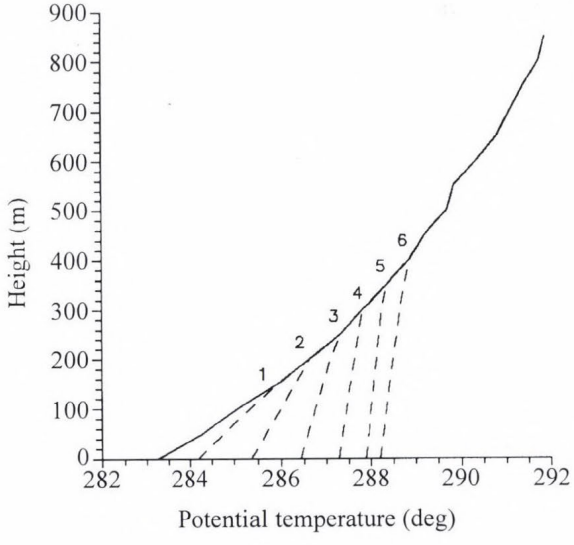

Fig. 5. As in Fig. 4 but for $k = 5$.

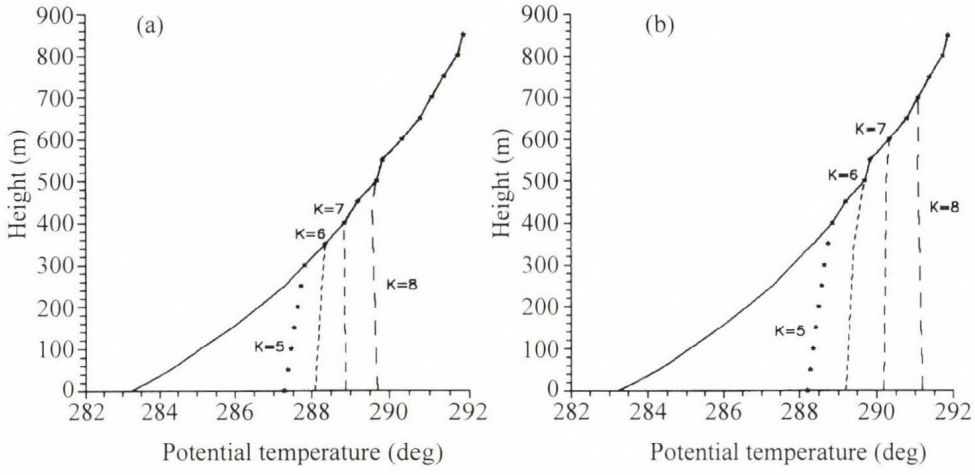

Fig. 6. Vertical profiles of horizontal-mean potential temperature for different magnitudes of radiation heating k = 5,6,7,8. (*a*) four hours after sunrise; (*b*) six hours after sunrise. The initial potential temperature profile, initial velocities, temperature excesses and size distribution of the thermals are as in Fig. 4.

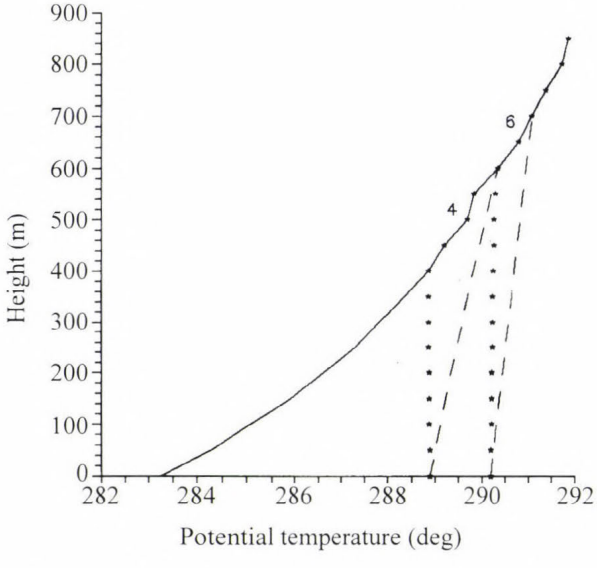

Fig. 7. Vertical profiles of horizontal-mean potential temperature for two types of size distributions of the thermals at the earth's surface 4 and 6 hours after sunrise. The type ST1 (asterisks) is given in Table 1 and type ST2 (dashed lines) — in the text. The initial potential temperature profile, initial velocities and temperature excesses of the thermals as well as the parameter k are as in Fig. 4.

To study the sensitivity of the model to the size distribution of thermals at the earth's surface the model was run for two types of size distributions — ST1 (see Table 1) and ST2. The results are presented on *Fig.* 7 where the calculated potential temperature profiles for four and six hours after sunrise are given. For the size distribution of type ST1, the potential temperature profiles are marked with asterisks, and for ST2 with dashed lines. In the case of the size distribution of type ST1, i.e. the heat is transported by thermals with diameters between 5 m and 128 m, for four and six hours after sunrise the potential temperature profiles are changed up to 400 m and 600 m, respectively. When the size distribution is of type ST2, i.e. the heat is transported by thermals with diameters 50–250 m, four and six hours after sunrise the changes in the potential temperature profile reach up to 600 m and 700 m, respectively. These results show that the bigger the ascending thermals initially are, the stronger they affect the initial temperature profile. This is due to the fact that larger thermals can ascend higher than smaller ones because the entrainment of the environmental air is smaller for them. The model results show that the CBL is not developed even six hours after sunrise in the case of the ST2 type distribution.

5. Summary and conclusion

A one-dimensional numerical model of evolving morning CBL has been developed. The basic idea of the model is that the heat in the convective mixed layer is transported by isolated buoyancy-driven turbulent eddies (thermals). Partitioning the CBL into 'updrafts' and compensating 'downdrafts' domains, the governing equation for the evolution of the horizontal-mean potential temperature was derived. This equation together with the initial and boundary conditions perform an unclosed initial value problem because its coefficients depend on unknown characteristics of the rising thermals as well as on their size distribution. The problem has been closed by assuming that thermals ascend as individual ones. Only vertical velocities, temperature excesses and size statistics of thermals at the earth's surface have to be given in order to compute numerically the evolution of the vertical profiles of the horizontal-mean potential temperature.

The model was run for two model initial temperature profiles in order to test its sensitivity to the initial sounding. These profiles correspond to nocturnal ground inversions. The calculations show that the CBL is formed in two stages. Initially the result of the increase of solar radiation is only the gradual decrease of the lapse rate of potential temperature and the gradual erosion of temperature inversion in a layer of growing thickness. During this stage — in the model two to three hours after sunrise — there is no CBL. The CBL as a layer with vanishing lapse rate of potential temperature is fully developed by four hours after sunrise and then its height grows. The CBL has the same type of evolution

for the case of a real initial sounding, too. Therefore the scenario of the convective mixed layer development qualitatively does not depend on the strength of the temperature inversion. The influence of the degree of the static stability of the initial temperature sounding changes only quantitatively the picture of evolution. As it could be expected, the stronger the initial temperature inversion, the lower the growth rate of the thickness of the layer affected by thermals in the first stage and the growth of CBL depth in the second stage. The same is valid for the heights of those layers a given time after sunrise.

A second type of numerical simulation was carried out by varying the parameter that controls the magnitude of radiation heating. The main result of the numerical tests is that there is a critical value of that parameter. When the magnitude of radiation heating is less than a critical value, the CBL is not formed, while when it takes values greater than the critical one there are fully formed convective mixed layers four hours after sunrise.

The model was run for two types of size distribution to study the sensitivity to the size statistics of thermals at the earth's surface. The calculation demonstrates physically adequate response of the model to the type of size statistics of thermals.

In conclusion, the numerical experiments indicate that in general the presented model gives reasonable results for the morning CBL evolution in the case of weak wind, absence of clouds and strong solar heating.

References

Andreev, V. and *Panchev, S.*, 1975: *Dynamics of Atmospheric Thermals* (in Russian). Gidrometeoizdat, Leningrad.

Andreev, V. and *Ganev, K.*, 1981: Model of convective heat exchange due to isolated thermals in the atmospheric boundary layer. *Boundary-Layer Meteorology 20,* 331-339.

Brunzov, H.T., Donev, E.H., Panchev, S., 1992: Experimental investigation of the structure and dynamics of temperature inversion and convective boundary layer above Sofia-area. Evaluation of the possibility of the apparatus available (in Bulgarian). *Ann. de L'Universite de Sofia 82,* 147-167.

Chatfield, R.B. and *Brost, R.A.*, 1987: A two-stream model of the vertical transport of trace species in the convective boundary layer. *J. Geophys. Res. 92,* 13263-13276.

Frish, S.A. and *Businger, J.A.*, 1973: A study of convective elements in the atmospheric surface layer. *Ibid. 2,* 301-328.

Hunt, J.C.R., Kaimal, J.C. and *Gaynor, J.E.*, 1988: Eddy structure in the convective boundary layer-new measurements and new concepts. *Quart. J. Roy. Meteorol. Soc. 114,* 827-858.

Lamb, R.G., 1982: Diffusion in the convective boundary layer. In *Atmospheric Turbulence and Air Pollution Modeling* (eds.: *F.T.M. Nieuwstadt* and *H. van Dop*). D. Reidel Hingham, Mass, 159-229.

Lenschow, D.H. and *Stephens, P.L.*, 1980: The role of thermals in the convective boundary layer. *Boundary Layer Meteorol. 19,* 509-532.

Lenschow, D.H. and *Stephens, P.L.*, 1982: Mean vertical velocities and turbulence intensity inside and outside thermals. *Atmos. Environ. 16,* 761-764.

Matveev, L.T., 1981: *Cloud Dynamics* (in Russian). Gidrometeoizdat, Leningrad.

Manton, M.J., 1975: Penetrative convection due to a field of thermals. *J. Atmos. Sci. 32*, 2272-2277.

Roisin, B., 1982: A theory of convection: Modeling by two buoyant interaacting fluids. *Geophys. Astrophys. Fluid Dynamics 19*, 35-59.

Telford, J.W., 1966: The convective mechanism in clear air. *J. Atmos. Sci. 23*, 652-666.

Telford, J.W., 1992: Clouds, noncloudy latent heat convection, entrainment, and horizontal averaging. *J. Atmos. Sci. 49*, 1848-1860.

Vulfson, N.T., 1961: *Convective Motion in a Free Atmosphere* (in Russian). Publ. Akad Nauk SSSR.

Warner, J. and *Telford, J.W.*, 1967: Convective below cloud base. *J. Atmos. Sci 24*, 374-382.

Young, G.S., 1988: Turbulence structure of the convective boundary layer. Part II; Phoenix 78 Aircraft Observations of Thermals and Their Environment. *J. Atmos. Sci 45*, 727-735.

IDŐJÁRÁS

Quarterly Journal of the Hungarian Meteorological Service
Vol. 101, No. 1, January–March 1997, pp. 17–31

Estimating probability density functions by kernel techniques

I. Matyasovszky

Department of Meteorology, Eötvös Loránd University,
Ludovika tér 2, H-1083 Budapest, Hungary; E-mail: matya@ludens.elte.hu

(Manuscript received 3 March 1996; in final form 4 October 1996)

Abstract—Kernel density estimation methods are discussed as flexible alternatives to traditional parametric methods for probability density estimation of climatological variables. Basic properties of such estimators are reviewed in this paper. The selection of the kernel function is outlined and attention is then focused on the bandwidth choice. Constant bandwidth and varying bandwidth kernel estimators are applied to daily mean temperature in Nebraska, USA. The histogram shows a possible complicated form of the probability density. The estimates are compared to each other and to a parametrically fitted binormal density. The results obtained demonstrate the usefulness of kernel estimators with local bandwidths.

Key-words: probability density function, kernel estimator, kernel function, bandwidth.

1. Introduction

Estimating probability distributions is a classical problem in meteorology. Parametric approaches which require an assumption on the type of the probability distribution are traditionally used for this purpose. Having a distribution type its parameters are estimated using one of several methods, like the maximum likelihood technique, or the method of moments. A review of frequently used distribution types can be found, for instance, in *Essenwanger* (1986).

Although well-developed statistical tests (e.g., the Kolmogorov-Smirnov test, or the chi-square test) can be used to check the fit of a selected distribution type, several important problems may arise. First, if a given distribution type fits observational data satisfactorily there is no guaranty that no other distribution type fits even better. In other words, since the true distribution is not known, just a best member of candidate distributions can be determined. However, it is not unusual that no particular distribution appears to be clearly

the best because the candidate distributions are close to each other and the goodness of fit measured by one of the common methods (e.g., chi-square norm, or entropy norm) cannot distinguish among those distributions. For instance, beside the two-parameter Weibull distribution (*Justus et al.*, 1976) the gamma and log-normal distributions (*Stewart* and *Essenwanger*, 1973) are generally used to model wind speed. A special case of this problem is when a distribution is compared with a more general class of distributions. For instance, the Rayleigh distribution having one parameter to be estimated is a special case of the Weibull distribution and under certain climate conditions the Rayleigh distribution can be used for wind speed (*Hennessey*, 1977). The necessity of a more general distribution can be analyzed by the likelihood ratio test, but frequently it is uncertain which type should be preferred.

Another problem is that a given meteorological element can follow different distributions depending on time. It is well-known that daily precipitation amount can be described by gamma distributions, but often, log-normal distributions are fitted for short time intervals (*Biondini*, 1975).

In several cases the variables in question appear to be poorly described by any of the distribution types discussed in even specialized statistical literature. For instance, hourly incoming global radiation was modeled by Weibull, log-normal, gamma, and chi-square distribution types (*Matyasovszky*, 1992), but none of these distributions could provide a fit consistent with observational data. In such cases transformations resulting in 'nicely behaving' variables can help the climatologist.

A further deficiency may be that standard distribution types (normal, log-normal, gamma, etc.) are unimodal, thus they cannot be applied to model multimodal distributions. A possibility to describe such distributions is to use mixtures of unimodal distributions. The probability density function $f(x)$ is then expressed as:

$$f(x) = \sum_{i=1}^{I} p_i f_i(x), \tag{1}$$

where p_i is the probability that the random variable comes from the ith distribution type and $f_i(x)$ is the probability density corresponding to that type. Using two-parameter distributions, which is the typical case, the number of parameters to be estimated is equal to $2I + (I - 1)$, a relatively large number even for small values of I.

The above mentioned difficulties establish the rationale of using non-parametric density estimators when no assumption is needed on the distribution to be estimated. The principle of these techniques introduced by *Rosenblatt* (1956) and *Parzen* (1962) is that each sample element x_i has a contribution to the density $f(x)$ and these contributions (weights) are proportional to the

distances between x and x_i. The weights are calculated through a so-called kernel function scaled by a smoothing parameter. This parameter controls how fast the weights decrease as the distances between x and x_i increase. An overall discussion of kernel density estimators can be found in *Silverman* (1986).

Mathematics of kernel density estimators have been mostly developed, but, according to our best knowledge, no meteorological application of these techniques has been reported. The purpose of this study is, therefore, to show the possibilities of this methodology. First the kernel density estimator is defined and its asymptotic properties are shown. The choice of a kernel and a smoothing parameter, key elements of applying kernel estimators, is discussed next. Since the role of the smoothing parameter seems especially crucial, we will focus on this question. Daily mean temperature in Nebraska, USA is used in Section 3 as an illustrative example for estimating bimodal distributions non-parametrically. Finally a brief section for discussion and conclusions is provided.

2. *Kernel density estimator*

The Parzen-Rosenblatt kernel density estimate $\hat{f}(x)$ from a sample $\{x_1, x_2, \ldots, x_n\}$ of size n is given by

$$\hat{f}(x) = \frac{1}{n}\sum_{i=1}^{n} \frac{1}{b} K\left(\frac{x - x_i}{b}\right), \tag{2}$$

where $K(z)$ is a so-called kernel function satisfying certain properties to provide an appropriate estimate of $f(x)$. The bandwidth b tends to zero as n tends to infinity.

A possibility for choosing the kernel is that $K(z)$ itself is a density function because $K(z)$ is required to integrate to unity. $K(z)$ with support [-1,1], i.e. $(K(z)_{[-1,1]})$ is called kernel of order k if the condition

$$\int_{-1}^{1} K(z) z^j dz = \begin{cases} 1, & j = 0, \\ 0, & 0 < j < k \end{cases} \tag{3}$$

is satisfied. Note that a density symmetric to zero is a second order kernel. The choice of $K(z)$ and b is discussed in the next section.

$\hat{f}(x)$ is an asymptotically unbiased and consistent estimate of $f(x)$ and the asymptotic mean square error (MSE) of the kernel density estimate Eq. (2) is given by

$$MSE[\hat{f}(x)] = E[(\hat{f}(x) - f(x))^2] = u^2(x) + v^2(x), \tag{4}$$

where the asymptotic bias is equal to

$$u(x) = E[\hat{f}(x) - f(x)] = B\frac{h^k}{k!}f^{(k)}(x) \tag{5}$$

and the asymptotic variance is

$$v^2(x) = Var[\hat{f}(x)] = E[(\hat{f}(x) - E(\hat{f}(x))^2] = \frac{V}{nb}f(x), \tag{6}$$

while

$$B = \int_{-1}^{1} K(z)z^k dz, \qquad V = \int_{-1}^{1} K^2(z)dz. \tag{7}$$

E denotes the expectation and $f^{(k)}$ is the kth derivative which is assumed to be finite. The dependence of the MSE on the density and its kth derivative, the kernel, and the bandwidth is clearly shown by Eqs. (3) to (6). The bias Eq. (5) is higher in areas where $f^{(k)}$ is higher, and the variance Eq. (6) is higher where $f(x)$ is large. The bias term penalizes oversmoothing, and the variance term penalizes undersmoothing. Thus an optimal b that recognizes this trade-off must exist. The optimal b minimizing MSE at a point x is

$$b_{opt} = \left(\frac{f(x)V}{(f^{(k)})^2 nB^2}\right)^{1/(2k+1)} \tag{8}$$

and the convergence rate of $\hat{f}(x)$ to $f(x)$ in terms of the integrated MSE (IMSE)

$$IMSE = \int_{-\infty}^{\infty} E\left[(\hat{f}(x) - f(x))^2\right]dx = \int_{-\infty}^{\infty} (u^2(x) + v^2(x))dx \tag{9}$$

is proportional to $n^{-2k/(2k+1)}$. The fastest convergence can be achieved by using b_{opt} which, however, cannot be determined in practice because it needs the knowledge of $f(x)$. The bandwidth, therefore, should be estimated from the sample.

One could think that the choice of b is not a difficult problem by using the bandwidth which delivers, in some sense, a best fit to the sample available,

while the choice of k and K seems to be highly arbitrary. However, the situation is just the contrary. A class of optimal kernel functions is known, and several simulation and real data studies suggest that a small variability in k does not considerably affect the resulting density. Generally, a relatively small value of k, say $k = 2$ can be chosen. In contrast, the choice of b has a great importance, and therefore we will focus principally on this question.

3. Kernel and bandwidth choice

3.1 Kernel choice

The choice of kernels is based on asymptotic properties Eqs. (5) and (6). The solutions of the variational problem

$$\int_{-1}^{1} K^2(z)\,dz \rightarrow \min \tag{10}$$

are called minimum variance kernels since they minimize the asymptotic variance Eq. (6). Such kernels can be found in *Gasser et al.* (1985). The minimum variance kernels are polynomials of even orders. For instance, for $k = 2$ and $k = 4$ the kernels are $K(z) = 1/2_{[-1,1]}$ and $K(z) = 3/8(3 - 5z^2)_{[-1,1]}$, respectively. *Müller* (1984) discussed a more general class of kernel functions which minimizes the asymptotic variance of the μth ($\mu \geq 0$) derivative of the kernel estimate. One of the most frequently used kernel is

$$K(z) = \frac{3}{4}(1 - z^2)_{[-1,1]} \tag{11}$$

with $k = 2$, $\mu = 1$. The above kernels, however, may be used just in the case when $f(x)$ is defined on the interval $(-\infty, \infty)$, unless the kernels are modified near the endpoints. *Gasser* and *Müller* (1979) defined boundary kernels with asymmetric support satisfying moment conditions necessary to maintain the order of unbiasedness in boundary intervals. Minimum variance kernels were derived by *Gasser et al.* (1985). *Müller* (1991) has developed a very general formulation to have kernels for any $x \in (m, M)$ and for any k, $\mu \geq 0$, where (m, M) denotes the support of $f(x)$. Let K_+ and K_- be functions with support [0, 1] $\times$ [-1, q] and [0, 1] $\times$ [-q, 1], respectively and with some smoothing requirements (*Müller*, 1991, p. 523). Then, kernels at a point x are given by

$$K_x(z) = \begin{Bmatrix} K_+(1,z), & b/(M-m) \le z \le 1 - b/(M-m) \\ K_+((x-m)/b,z), & 0 \le z < b/(M-m) \\ K_-((M-x)/b,z), & 1 - b/(M-m) < z \le 1 \end{Bmatrix},$$

where $K_-(q, z) = K_+(q, -z)$ and $q = 1$ for $x \epsilon [m + b, M - b]$ (interior), $q = (x - m)/b$ for $m \le x < m + b$ (left boundary region), $q = (M - x)/b$ for $M - b < x \le M$ (right boundary region). Eq. (7), necessary to calculate the asymptotic bias and variance, essentially holds, but now B and V depend on q (see *Müller*, 1991, p. 523). For $k = 2$, $\mu = 1$, and in the interior region of the support of $f(x)$ ($q = 1$) $K_x(z)$ becomes Eq. (11).

3.2 Bandwidth choice

Constant bandwidth. In parametric density estimation the parameters are estimated by maximum likelihood, least squares, or other methods. A natural way to estimate bandwidth is, therefore, to use these concepts for kernel estimators.

A direct application of the maximum likelihood principle is unsuccessful, since the degenerate choice of $b = 0$ maximizes the likelihood function. Therefore, a maximum likelihood cross-validation (MLCV) version developed by *Habbema et al.* (1974) can be offered for this purpose. The bandwidth b is chosen by maximizing a cross-validated likelihood function defined as

$$\prod_{i=1}^{n} \hat{f}_i(x_i),$$

where $\hat{f}_i(x_i)$ is the kernel density estimate at x_i with the x_i omitted. Substituting $\hat{f}_i(x_i)$ into the likelihood function, the

$$MLCV = \prod_{i=1}^{n} \left[\frac{1}{n-1} \sum_{j \neq i}^{n} \frac{1}{b} K\left(\frac{x_i - x_j}{b} \right) \right] \tag{12}$$

is obtained to be maximized with respect to b. A major theoretical study of the properties of MLCV is presented in *Hall* (1987).

The least square method for estimating b based on a minimization of the IMSE was suggested by *Rudemo* (1982). Given an estimator $\hat{f}(x)$, the IMSE can be written as

$$\int_{-\infty}^{\infty}(\hat{f}(x) - f(x))^2 dx = \int_{-\infty}^{\infty}\hat{f}^2(x)\,dx - 2\int_{-\infty}^{\infty}\hat{f}(x)f(x)\,dx + \int_{-\infty}^{\infty}f^2(x)\,dx.$$

The last term of the above equation does not depend on b and the first term can be estimated directly from the estimate $\hat{f}(x)$. It can be shown that the expectation of the second term is equal to

$$2/n \sum_{i=1}^{n} \hat{f}_i(x_i).$$

The data-based LSCV to be minimized to choose b is then

$$LSCV = \int_{-\infty}^{\infty}\hat{f}^2 dx - 2/n \sum_{i=1}^{n} \hat{f}_i(x_i),$$

which is generally approximated by

$$LSCV = 1/n \sum_{i=1}^{n} \hat{f}^2(x_i) - 2/n \sum_{i=1}^{n} \hat{f}_i(x_i), \tag{13}$$

where

$$\hat{f}_i(x_i) = \frac{1}{n-1} \sum_{j \neq i} \frac{1}{b} K\left(\frac{x_i - x_j}{b}\right).$$

Hall and *Marron* (1987) demonstrated the optimality of LSCV for density estimation in terms of IMSE. They showed that no other cross-validation bandwidth selection procedure can deliver smaller IMSE than LSCV. This is the reason why LSCV is preferred in almost every application. However, even this best bandwidth estimator has serious limitations. Specifically, the relative convergence rate of the estimated bandwidth to the optimal bandwidth is only proportional to $n^{-1/10}$ (*Hall* and *Marron*, 1987). For this reason, considerable effort has been put forth to find more accurate practical methods (see e.g. *Marron*, 1989). An important class of improved bandwidth selectors includes the so-called plug-in methods. A plug-in estimator is constructed in two steps: first, an initial estimate $\hat{f}(x)$ called pilot estimate is calculated using a bandwidth obtained from LSCV (Eq. 13); then, this estimate is plugged into IMSE (Eq. 9) substituting $f(x)$ and $f^{(k)}(x)$ by $\hat{f}(x)$ and $\hat{f}^{(k)}(x)$, respectively and IMSE is minimized with respect to b. $\hat{f}^{(k)}(x)$ can be approximated numerically

from $\hat{f}(x)$ using a finite difference scheme. Such an estimator can reach a relative convergence rate of $n^{-1/2}$ (e.g. *Hall et al.*, 1991), the fastest possible convergence rate of bandwidth estimation (*Hall* and *Marron*, 1987). Another class of improved bandwidth selectors utilizes frequency domain representation of LSCV. A modification of LSCV using some cut-off frequency filters the high frequencies out from the estimator and delivers a relative convergence rate of $n^{-1/2}$ (*Chiu*, 1992).

Plug-in estimators suggest the use of local bandwidths, because instead of minimizing IMSE a minimitazion of MSE for every particular x results in locally varying bandwidths.

Local bandwidth ($b(x)$). MSE of $\hat{f}(x)$ is governed by $f(x)$ and $f^{(k)}(x)$ (Eqs. (4) to (7)). This fact motivates the choice of locally varying bandwidths. A smaller bandwidth near the peaks of $f(x)$ reduces the bias and a larger bandwidth in the flat regions of $f(x)$ reduces the variance. Therefore, it may be expected that a good strategy for choosing local bandwidth $b(x)$ yields smaller IMSE than the IMSE of ordinary bandwidth selection for global bandwidth b.

In general, the construction of a local bandwidth estimator entails a two-step procedure. The first step produces a pilot estimator using a fixed bandwidth and the second step yields the local bandwidth estimator. This second step requires a reformulation of Eq. (2). Since the bandwidth b may depend on either x or x_i two versions of kernel estimators are discussed

$$\hat{f}_1(x) = \frac{1}{n} \sum_{i=1}^{n} \frac{1}{b(x)} K\left(\frac{x - x_i}{b(x)}\right) \tag{14}$$

$$\hat{f}_2(x) = \frac{1}{n} \sum_{i=1}^{n} \frac{1}{b(x_i)} K\left(\frac{x - x_i}{b(x_i)}\right). \tag{15}$$

An important disadvantage of the first estimator is that $\hat{f}_1(x)$ typically does not integrate to unity and thus is usually not itself a density. A further disadvantage is that no specification of $b(x)$ can be stated automatically. The second estimator is used in a form $b(x_i) = hf^{-1/2}(x_i)$ because this choice eliminates the asymptotic bias of Eq. (15). Then $\hat{f}_2(x)$, called Abramson estimator (*Abramson*, 1982), is equal to

$$\hat{f}_2(x) = \frac{1}{n} \sum_{i=1}^{n} \frac{f^{1/2}(x_i)}{h} K\left(\frac{(x - x_i) f^{1/2}(x_i)}{h}\right), \tag{16}$$

where h is a parameter to be estimated. The asymptotic IMSE of $\hat{f}_1(x)$ and $\hat{f}_2(x)$ is expected to be smaller than or at most equal to IMSE of fixed bandwidth estimators. Indeed, a frequently used version of $\hat{f}_1(x)$ was found to

be more efficient than the fixed bandwidth estimator, but it allows very little improvement (*Terrel* and *Scott*, 1992). $\hat{f}_2(x)$ exhibits larger asymptotic IMSE than the fixed bandwidth estimator, because the estimate at a point x can be strongly influenced by points x_i far from x. In spite of this fact the Abramson estimator is preferred in practice because it enjoys a significant reduction of IMSE for small and moderate sample sizes. Such sample sizes represent the typical case in climatology. The efficiency of the Abramson estimator over fixed bandwidth estimators seems to disappear only for sample sizes of ten thousands (*Terrel* and *Scott*, 1992).

The parameter h in Eq. (16) can be estimated by cross-validation as described by *Hall* (1992). The quantity to be minimized to choose h is

$$CV = 1/n \sum_{i=1}^{n} \tilde{f}_2^2(x_i) - 2/n \sum_{i=1}^{n} \tilde{f}_2(x_i), \tag{17}$$

where

$$\tilde{f}_2(x) = \frac{1}{n} \sum_{j=1}^{n} \frac{\check{f}_j^{1/2}(x_j)}{h} K\left(\frac{(x_i - x_j)\check{f}_j^{1/2}(x_j)}{h} \right) \tag{18}$$

is the Abramson estimate at x_i with a cross-validated constant bandwidth pilot estimate

$$\check{f}_i(x_i) = \frac{1}{n-1} \sum_{j \neq i} \frac{1}{b} K\left(\frac{x_i - x_j}{b} \right). \tag{19}$$

However, as the performance of cross-validation for estimating fixed bandwidth is relatively poor, so is for estimating h. *Müller* and *Wand* (1990) and *Müller* and *Zhou* (1991), therefore, proposed the following procedure. The bias $u(x)$ and the variance $v^2(x)$ of the estimator (14) can be rewritten as:

$$u(x) = \int_{-\infty}^{\infty} K(z) f(x - b(x)z)\, dz - f(x) \tag{20}$$

$$v^2(x) = \frac{1}{nb(x)} \int_{-\infty}^{\infty} K^2(z) f(x - b(x)z)\, dz. \tag{21}$$

The local bandwidth is estimated by minimizing the expression

$$MSE(x) = u^2(x) + v^2(x) \tag{22}$$

with substituting $f(x)$ in Eqs. (20) and (21) by a pilot estimate. This minimization of (22), referred to as Müller estimator, does not use asymptotic expressions, but rather the exact MSE is estimated and then minimized. It was shown in *Müller* and *Wang* (1990) that, for a large range of pilot bandwidths, the estimated local bandwidth converges to the optimal local bandwidth in terms of MSE.

4. Example

Daily mean temperature in Nebraska, USA for January is examined using a data set for the period from 1950 to 1989. To analyze the probability distribution a statistically independent sample is needed, but daily temperatures are serially correlated. Therefore, a temperature subset has been created picking up each fifth temperature value from the original data set, since autocorrelations for lags larger than four or five days are quite small (*Fig. 1*). Thus, an approximately independent sample of size $n = 280$ is available for daily mean temperature.

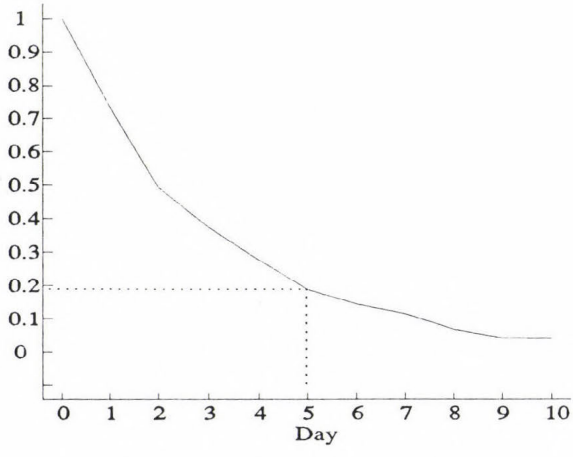

Fig. 1. Autocorrelations of daily mean temperature at Grand Island, U.S. in January.

Fig. 2 shows the histogram of this subsample of daily mean temperature at Grand Island. Even a visual examination suggests that a normal distribution commonly used to describe temperatures does not fit. Indeed, either a Chi-square test or a Kolmogorov-Smirnov test rejects the hypothesis that the temperature follows a normal distribution even at the 99% significance level. The distribution seems to be quite asymmetric or even bimodal. One mode of the histogram appears at relatively high temperatures, while the second and smaller

mode corresponds to very low temperatures. This second mode is associated with strong northern advection of cold air masses ('North Pole Express').

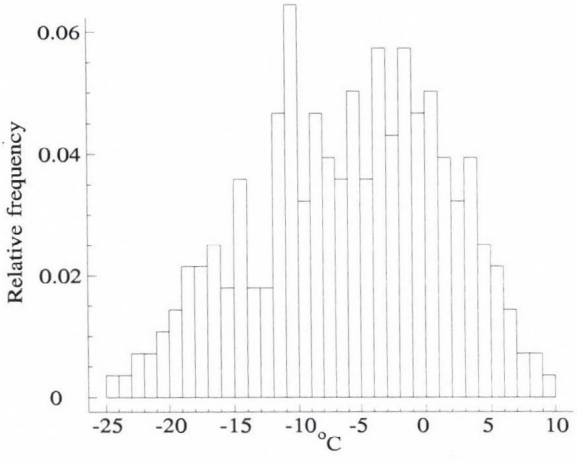

Fig. 2. The histogram of daily mean temperature at Grand Island, U.S. in January.

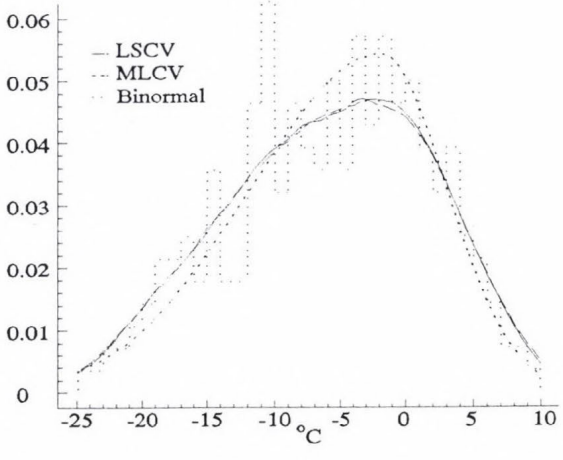

Fig. 3. Probability density function of daily mean temperature estimated with maximum likelihood (MLCV) and least square (LSCV) cross-validated bandwidths.

First the MLCV and LSCV techniques have been used with kernel Eq. (11) and nearly the same bandwidths have been obtained. According to the bandwidths $b = 5.4°C$ (LSCV) and $b = 5.9°C$ (MLCV) the corresponding densities are almost identical as it is seen in *Fig. 3*. In an earlier examination

(*Matyasovszky et al.*, 1994), a binormal distribution has been used to model daily mean temperature in Nebraska. The binormal distribution is similar to the Gaussian except for its symmetry as discussed in *Toth* and *Szentimrey* (1990). This density function indicated in Fig. 3 differs substantially from the two nonparametric estimates. This may be a consequence of the inadequacy of the binormal distribution model, or the inadequacy of using constant bandwidths for nonparametric estimation. Nonparametric estimates look overestimated at flat regions of $f(x)$, and underestimated at the peak regions.

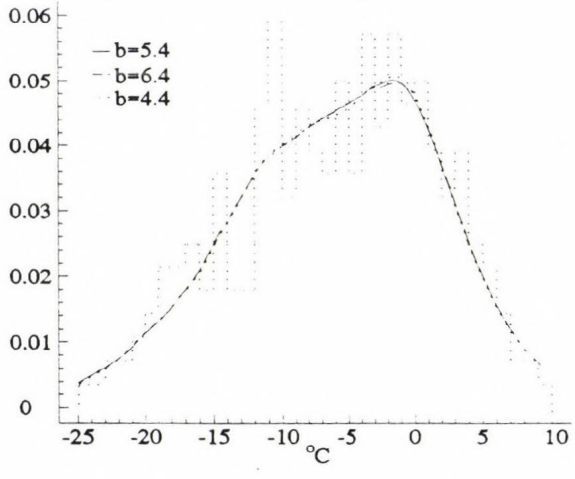

Fig. 4. Probability density function of daily mean temperature estimated by the Abramson method

A deeper analysis, therefore, should apply local bandwidths. *Fig. 4* shows the Abramson estimate of the probability density using pilot estimate with the bandwidth ($b = 5.4$°C) obtained from LSCV. Two other curves are indicated corresponding to pilot bandwidths somewhat larger and smaller than the LSCV-selected bandwidth. The three density functions seem identical which demonstrates the robustness of the Abramson estimator in view of different pilot estimates. The asymmetry of the density is considerably larger than in the constant bandwidth case. The location of the maximum corresponds to the expected principal mode, and a relatively strong increase of the curve is experienced at temperatures –15 to –10 °C, but no second mode has appeared. The Müller estimates show a finer structure of the underlying density, the second mode has formed clearly (*Fig. 5*).

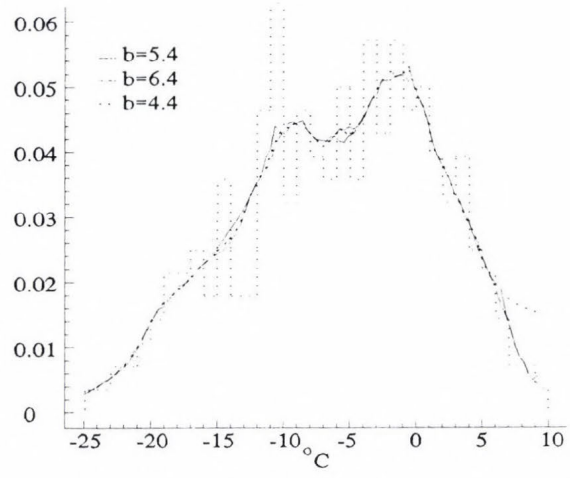

Fig. 5. Probability density function of daily mean temperature estimated by the Müller method.

5. Discussion and conclusions

First, two classical bandwidth selectors, namely the maximum likelihood and least square cross-validation were used to estimate probability density of daily mean temperature at Grand Island, Nebraska in January. The obtained densities are close to each other, but considerably different from a parametrically fitted binormal density (Fig. 2). Nonparametric estimates look overestimated at the flat regions of the density, and underestimated at the peak regions. Therefore, stabilized ($n^{-1/2}$ convergent) constant bandwidth selectors were not applied here since the use of local bandwidths seemed more promising. Figs. 3 and 4 strengthen the theoretical finding, namely: the Abramson and Müller estimators are robust in respect to the bandwidths used in pilot estimates. The only but important drawback to the present application example is that the two above techniques resulted in substantially different estimates. Which estimate can be rather believed ?

To answer this question a stronger knowledge of the properties of nonparametric density estimators is necessary. Three important and useful tools for understanding the behavior of these estimators include the asymptotic analysis, simulation and numerical calculation of one of the error criteria, like IMSE. The strength of asymptotic analysis is that it gives general results for each possible density. It is not known, however, how a given sample size is close to sizes where the behavior of a specific estimate can be substituted by the asymptotic behavior. By simulating samples of size n corresponding to a given density and by calculating kernel estimate for each simulated sample, the

properties of the estimator can be evaluated. The weakness of this process is that the results obtained are applicable only to the densities and sample sizes used in the simulation. The numerical calculation of error criteria seems to be the most promising approach to analyze the behavior of kernel estimators. The main idea is the exact calculation of error criteria for special classes of examples which make the calculation tractable, but at the same time represent a broad base of cases. *Marron* and *Wand* (1992) defined several classes of densities as mixtures of normal densities. The family of normal mixture densities is very flexible and the formulae derived allow exact analysis for a wide variety of density shapes. One of the most important findings is that the practical importance of higher order kernels is surprisingly small. This is the reason why only the order $k = 2$ was applied in this paper. Another important result is that the usual asymptotic approximation to IMSE can be quite inaccurate, especially when the underlaying density is not 'too smooth'. These conclusions were drawn for constant bandwidths, but similar, although less general findings have been obtained for local bandwidth case (*Terrel* and *Scott*, 1992; *Hall*, 1992).

Considering the above facts, my feeling is that the Müller estimator provides the better estimate in the present application case since the Müller estimate is based on an exact expression of MSE, while the choice of $b(x_i)$ in Eq. (15) resulting in the Abramson estimator Eq. (16) is based on the asymptotics of Eq. (15).

Acknowledgements—Much of this work was completed while the author was at the Department of Civil Engineering, University of Nebraska, NE 68588. Research leading to this paper has been partly supported by grants from the U.S. National Science Foundation, EAR-9205717, and the Great Plains Regional Center of the National Institute for Global Environmental Change.

References

Abramson, I.S., 1982: On bandwidth estimation in kernel estimators — A square root law. *Ann. Statist. 10*, 1217-1223.

Biondini, R.W., 1975: The log-normal distribution and cumulus clouds. *Proc. Fourth Conf. on Prob. and Stat. in Atm. Sci.*, 76-79.

Chiu, S.T., 1992: An automatic bandwidth selector for density estimation. *Biometrika 79*, 771-782.

Essenwanger, O.M., 1986: *General Climatology, 1B: Elements of Statistical Analysis. World Survey of Climatology*. Elsevier, Amsterdam-London-New York-Tokyo.

Gasser, T. and *Müller, H.G.*, 1979: Kernel estimation of regression functions. *Lecture Notes in Mathematics 757*, 23-68.

Gasser, T., Müller, H.G. and *Mammitzch, V.*, 1985: Kernels for nonparametric curve estimation. *Quart. J. Roy. Statist. Soc. B. 47*, 238-252.

Habbema, J.D.F., Hermans, J. and *Broek, V.D.*, 1974: A stepwise discrimination program using density estimation. In *Compstat* (ed.: *G. Bruckman*). Physica Verlag, Vienna.

Hall, P., 1987: On Kullback-Leibler loss and density estimation. *The Annals of Statistics 15*, 1491-1519.

Hall, P. and *Marron, J.S.*, 1987: Extent to which least squares cross-validation minimizes integrated squared error in nonparametric density estimation. *Prob. Theory Rel. Fields 74*, 567-568.

Hall, P., Sheather, S.J., Jones, M.C. and *Marron, J.S.*, 1991: On optimal data-based bandwidth selection in kernel density estimation. *Biometrika 78*, 263-269.

Hall, P., 1992: On global properties of variable bandwidth density estimators. *The Annals of Statistics 20*, 762-778.

Hennessey, J.J. 1977, Some aspect of wind power statistics. *J. Appl. Met. 16*, 119-128.

Justus, C.G., Hargraves, W.R. and *Yaclin, Y.*, 1976: Nationwide assessment of potential output from wind power generators. *J. Appl. Met. 15*, 673-678.

Marron, J.S., 1989: Automatic smoothing parameter selection: a survey. *Empir. Econ. 13*, 187-208.

Marron, J.S. and *Wand, M.P.*, 1992: Exact mean integrated squared error. *The Annals of Statistics 20*, 712-736.

Matyasovszky, I., 1992: Simulation of hourly incoming global radiation. In *Constructing a Typical Meteorological Year* (ed.: *G. Major*) (in Hungarian). *OMSZ Series*, 68, Budapest, Hungary.

Matyasovszky, I., Bogardi, I., Bardossy, A. and *Duckstein, L.*, 1994: Local temperature estimation under climate change. *Theor. Appl. Climatol. 50*, 1-13.

Müller, H.G., 1984: Smooth optimum kernel estimates of densities, regression curves and modes. *The Annals of Statistics 12*, 766-774.

Müller, H.G., 1991: Smooth optimum kernel estimators near endpoints. *Biometrika 78*, 521-530.

Müller, H.G. and *Wang, J.L.*, 1990: Locally adaptive hazard smoothing. *Prob. Theor. Rel. Fields 85*, 523-538.

Müller, H.G. and *Zhou, H.*, 1991: Comments on *Transformations in Density Estimation* by *M.P. Wand, J.S. Marron* and *D. Ruppert. J. Am. Stat. Assoc. 86*, 356-358.

Parzen, E., 1962: On the estimation of probability density function and mode. *Ann. Math. Statist. 33*, 1065-1076.

Rosenblatt, M., 1956: On some nonparametric estimates of a density function. *Ann. Math. Statist. 27*, 832-837.

Rudemo, M., 1982: Empirical choice of histograms and kernel density estimators. *Scand. J. Stat. 9*, 65-78.

Silverman, B.W., 1986: *Density Estimation for Statistics and Data Analysis*. Chapman and Hall, London.

Stewart, D.A. and *Essenwanger, O.M.*, 1973: Frequency distribution of wind speed near the surface. *J. Appl. Met. 17*, 1633-1642.

Terrell, G.R. and *Scott, D.W.*, 1992: Variable kernel density estimation. *The Annals of Statistics 20*, 1236-1265.

Toth, Z. and *Szentimrey, T.*, 1990: The binormal distribution: A distribution for representing asymmetrical but normal-like weather elements. *J. Climate 3*, 128-136.

IDŐJÁRÁS

Quarterly Journal of the Hungarian Meteorological Service
Vol. 101, No. 1, January–March 1997, pp. 33–43

Air quality simulation models in Poland

Anna Madany

Warsaw University of Technology,
ul. Nowowiejska 20, 00-653 Warsaw, Poland
E-mail: madany@jowisz.iis.pw.edu.pl

(Manuscript received 1 August 1996; in final form 17 October 1996)

Abstract—The paper is a review of the air pollution dispersion models developed and used in Poland over the recent 15 years. Information about these models has been collected on an inquiry basis. Characteristics of these models, input data, problems of model verification and uncertainty of modeling are extensively described and presented in a Polish paper (*Madany* and *Bartochowska*, 1995). This article presents a brief summary of the most essential information about these models as a supplement to *Szepesi*'s Compendium (*Szepesi*, 1989).

Key-words: environmental protection, air pollution model, air pollution control, meteorological modeling uncertainty, dispersion model classification.

1. Introduction

Mathematical models of air pollution dispersion have been developed worldwide for over three decades now. Apart from their analytical aspect, models are essential environmental quality management instruments. They are used, for example, in developing warning systems and in identifying areas of risk in case of random emission occurrence, such as nuclear explosions or failure of nuclear power plant. Recently they have been incorporated into the so-called 'integrated models' geared to analyses of specific scenarios of pollution emission abatement and to cost and environmental impact analyses including *(Juda-Rezler et al.* 1996). Modeling with the use of the so-called influence function are also of substantial importance since they allow the identification of sources — even distant ones — which contribute most to the contamination of a specific, usually protected area (*Uliasz,* 1993).

The Compendium of Regulatory Air Quality Simulation Models of *Szepesi* (1989) presents about 700 papers from all over the world, but models from Poland are not comprised therein. This fact was the reason for writing this article. Information about models developed and used in Poland has been

collected by means of inquiries sent out to interested parties. Responses were returned by 12 centers, which presented 29 models developed by as much as 50 persons. The authors mainly are scientists of Polish Universities: Warsaw University of Technology, Jagiellonian University of Cracow, Warsaw University, Military University of Technology and large public institutions: Polish Academy of Sciences, Institute of Meteorology and Water Management, Central Laboratory of Radiation Protection and several private companies. (*The respondents' addresses are available from the author, Warsaw University of Technology, ul. Nowowiejska 20, 00-653 Warsaw, Poland.*)

Air pollution modeling is performed by people of various educational backgrounds and profiles, biased by a specific recognition of the phenomena and processes described. However, this problem branch requires the co-operation of various experts representing various scientific disciplines.

2. General model characteristics

A comprehensive description of a large number of models requires ranking under an adopted classification. This is not simple since the models differ from each other in various aspects: mathematical structure, the description (or a lack of that) of the physical state and physical processes within the gaseous medium of pollution dispersion, simplifications adopted in the modeling, the purpose, temporal and spatial scale, topographical conditions, quantity and quality of input data. Air pollution model classifications presented in the literature (*Sorbjan*, 1989; *Juda-Rezler,* 1991; *Szepesi,* 1989; *Venkatram* and *Seigneur*, 1993) differ substantially and simultaneously clarify the extensive diversity of the mathematical description of this problem. *Table 1* presents some basic information about the Polish models. This shall only become usable after discussing certain terms comprised therein. The temporal scale of modeling is of essential meaning, because short-term forecasting models, for computing instantaneous values of pollution concentrations 12 or 24 hours in advance, must differ in the level of detail and structure from a climatological model, defining monthly mean or annual mean concentrations. The spatial scale of the modeled area is also a distinguishing feature.

Commonly known as the *turbulent diffusion equation* is the basis for the majority of pollution dispersion models. It is derived from the mass conservation principle for pollutant concentration (C). In this equation variables C and V (wind) are averaged values depending on the averaging time. Atmospheric turbulence has a wide energy spectrum comprising various scales of movement. Therefore the interpretation of computation and survey results should account for this fact. One of the simplest ways of parameterization of turbulent fluxes from this equation by averaged variables is to adopt the hypothesis of proportionality of pollution mass turbulent flux $\overline{F}_c$ to concentration gradient:

$\vec{F}_c = -\hat{K}\nabla C$ where $\hat{K}$ is a tensor with nine components. This approximation (the so-called 'first-order-turbulent closure') defines the turbulent fluxes at the given point with the use of mean pollution concentration gradients (K-theory). In the majority of such models it is assumed that the $\hat{K}$ tensor has non-zero components only along the main diagonal. Sometimes it is also assumed that it is constant in time and space, but measurements show that K depends on the scale of turbulence, turbulent energy, the atmospheric equilibrium and land configuration. These models are useless for the description of dispersion during convection, strongly unstable conditions and within front areas.

The turbulent diffusion equation is a second-order parabolic partial differential equation. The adoption of a number of assumptions and approximations allows an analytical approach, exemplified by the Pasquill model of 1961, widely used in engineering practice. The model defines the so-called Gaussian Plume Model. Plume dispersion is defined by the dispersion coefficients σ_y and σ_z, depending on the distance traveled by molecules at atmospheric equilibrium state. It is determined in classes as a function of wind velocity at 10 m altitude and insolation. However, such approximation neglects the vertical structure of the atmosphere and comprises an excessive range of atmospheric conditions into the inert equilibrium and thus it is applicable for flat surface and horizontally homogeneous meteorological fields. It was further assumed that pollution does not undergo any chemical changes, there is no gravity fall, the plume reflects at the ground and is not absorbed thereby. These assumptions substantially reduce the extent of model applicability. The Gaussian Segmented Plume Model is a modification of the Pasquill equation for non-stationary emission and meteorological conditions (*Markiewicz,* 1994). The non-linear diffusion equation in full form (when the wind and turbulence coefficients are functions of the co-ordinates) requires numerical integration. Integration schemes using finite differences were most commonly used, however this method is only applicable for surface or volumetric emission sources of large sizes as compared with the numerical grid integration step. These obstacles can however be eliminated by a finite element scheme of integration of areas in the vicinity of point emission sources. Recently spectral methods have also been used in Polish models *(Bartnicki*, 1994).

Numerical integration of coupled diffusion equations allows two-variant source or receptor-oriented computations of pollution concentrations (*Uliasz,* 1993). This technique will be described as follows: modeling is geared to the determination of a certain characteristic of concentration at the given receptor $\phi(C)$, which may be generally defined as the $C(r,t)$ concentration integral in time and space of the modeled area:

$$\phi(C) = \int\int RC\,dt\,d\vec{r} = \int\int C^* Q\,dt\,\vec{dr}, \tag{1}$$

where C^* is the influence function, Q is the source output of pollutant emission, R is the receptor function (geometry and location of source). Traditional source-oriented computations consist of the forward integration of the diffusion equations in respect of time for given emission sources, to obtain a $C(r,t)$ concentration over the time and space modeling domain. The $C^*(r,t)$ influence function for a given receptor is obtained by the backward integration of the coupled diffusion equation in respect of time. C^* depends on the meteorological conditions, dry and wet deposition and transformations of pollution in the atmosphere, but it does not depend on the emission sources. It should be noted that the computative capacity of such an option is limited to linear dispersion models.

The *Eulerian model* is the most frequently used one in atmospheric dynamics; it presents the field of velocity $V = f(r,t)$, variables in space (r) and time (t) at each point of the studied area in a spherical or in a Cartesian coordinate system (x,y,z), fixed with respect to the ground. This model allows the incorporation of complex processes, e.g. non-linear chemical reactions. In Eulerian model assumptions the emission value is averaged within the grid cell, resulting in an overestimation of the concentration values in the vicinity of the emission source. *Lagrangian models* are based on relationships betwen coordinates of all considered particles and time and their initial location. *Lagrangian Particle Dispersion Models* (LPD) have recently become an important tool for pollution dispersion investigation. They are based on the assumption that atmospheric diffusion may be modeled with the use of Markov chains (*Uliasz,* 1993). It should be noted that mesoscale modeling of dispersion is much more difficult than modeling at local scale, since both the mean and turbulent flow characteristics are non-stationary and non-homogeneous in mesoscale. Such conditions exclude the use of small-scale diffusion models based on Gaussian distribution or probability mathematics. In LPD models dispersion is modeled by the simulation of the movement of a large number of molecules at amounts proportional to the pollutant emission concentrations. These molecules are simultaneously or successively transported by the wind. In these models wind velocity components u_i and its turbulent fluctuations u'_i are obtained from the meteorological model (preprocessor), complex enough to forecast turbulent components of velocity, variances, covariances and Lagrangian R_i correlations. The disadvantages of the Lagrangian methods are the inability to model nonlinear pollution change processes and the high cost of computer computations. For larger areas *hybrid Lagrangian-Eulerian models* are used *(Uliasz,* 1993).

The double stochastic model introduced by Polish mathematicians (*Kazimierczyk et al.*, 1993) forecasts the nitric oxides concentration fields. Nitric oxides (NO_x) undergo complex changes in the atmosphere, they disappear and reappear at random, hence $NO_{x\ molecule}$ trajectories are discrete. In this paper these phenomena are defined in two planes of calculus of probability, one for microscopic processes, the other for macroscopic ones.

Table 1. Collection and description of models

1	2	3	4	5	6	7	8	9	10	11	12
No.	Acronim	Model class	Model design	Dimen-sion, scale	Type of sources	Modeled pollutant	Physical & chemical processes	Meteorological data		Other input data	Refer-ences
								General inf.	Para-meters		
1.	AIREM	Gaus	diag	2D local	point volum	rad	wash, dep, chem	clima	v, H, γ, d	radde	[6]
2.	ALINA	grid, Eul	diag, exp-rep	1D local	area	cool.tower plume, dust	physical	prepr, own, mesurements	T, v, γ, p, f	emi, pars	[8]
3.	KZMA	Gaus	diag, prog	reg	point, area	SO_2	dep, chem	clima	v, γ	emi, pars, k	[10]
4.	MDMS	grid, Lgr, Eul	reas, diag, prog	3D reg	point, area, line	SO_2	dep	prepr	T, v, p, f, N, othem	emi, top, pars, z_o, veg, soil	[24] [25]
5.	MCHGIG	grid, Psq	diag, prog	3D reg	point, area, volum	rad-dust	dep	stand	T, v, γ, H, p, N	emi, imi, othes	[28]
6.	MKOAS	grid, Eul, Psq	prog, exp.rep	3D local,	point	dust, SO_2, NO_2	dep, chem	stand, clima	T, v, γ, H, p, N	emi, top, othin	[29]
7.	MOD	grid, Eul, 3lay	diag	2D, reg, local	point, area	SO_2, SO_4	dep, chem	prepr, stand, field	v, T, γ	emi, τ_d, pars, k, z_o, v_d	[11]

1	2	3	4	5	6	7	8	9	10	11	12
8.	SPM	Gaus, Psq, segpl	diag, reas	reg, local	point	dust, SO_2, NO_x	wash, dep, chem	stand, field	v, H, γ, T, d	emi, s_o, v_d pars, λ, z_o	[17]
9.	OSMA	grid, Eul, spect	diag, oper	3D macro	area	SO_2, SO_4	wash, dep, chem	prepr, stand	v, H, d	emi, k, λ, τ_d, v_d	[2]
10.	POLIGW	grid, Eul Psq	diag, prog	3D local	point, line	–	–	stand	T, v, γ	emi, imi, othin	[3]
11.	RAPFOS	grid, Lgr, Eul, two preproc.	diag, prog Izerskie Montain	3D reg	point, line, area	SO_2	dep, wash	prepr	T, p, v, N, f, d, othem	emi, pars, z_o, othin	[15]
12.	REGFOR3	grid, Eul	prog	2D reg, 3lay	point, line, area	SO_2, dust	wash, dep, chem	prepr	v, γ, H, d	emi, v_d, pars, s_o, k, z_o, top	[9]
13.	REGSIM	Gaus, Psq	exp-rep	reg	point, area	dust, SO_2, NO_x	wash, dep, chem	clima	T, v, γ, H, d	emi, z_o, k, pars, λ, v_d	[4]
14.	REMOTA	grid, Eul, spect	diag, oper	2D reg	point, line	hamet	wash, dep	stand	v, d	emi, λ, v_d	[7]
15.	SO2.ARX	stat	prog, oper	local	area	SO_2	–	prepr	T, v	imi	[18]
16.	SOXNOX	grid, Eul K-theory	diag	2D reg	point, area	SO_2, NO_x, NH_3, SO_4	wash, dep, chem	prepr, stand	H, v, d, T	pars, λ, v_d, z_o, s_o, τ_d, k	[1]
17.	DOUBLY STOCH	grid, doubstoch	prog, diag	3D reg	point, line, area	NO_x	wash, dep, chem	prepr, clima, stand, field	T, v, γ, H, d, N	emi, imi, k, v_d, top	[14]

1	2	3	4	5	6	7	8	9	10	11	12
18.	STOCH	grid, Eul, Kalm	prog, diag	3D, reg, local	point, area	SO_2	wash, dep, chem	prepr, clima, stand, field	T, v, γ, H, d	emi, imi, k, v_d, top	[23]
19.	URFOR2	Gaus, Psq	diag, reas	local	point, area	SO_2,	wash, dep, chem	field	T, v, γ, H, d	emi, pars, λ, k, v_d, z_o, s_o	[5]
20.	URFOR3	grid, Eul	prog	2D local 3lay	point, line, area	SO_2, dust	wash, dep, chem	prepr	v, γ, H, d	emi, pars, s_o, k, top, v_d, z_o	[9]
21.	WDSW2G	Gaus, Eul, Psq	diag exp-rep	3D local	point, line	-	-	stand	T, v, γ	emi, imi, othin	[3]

Symbols and denotations:

area - area; **chem** - chemical reactions; **clima** - climatological; **cool.tower plume** - cooling tower plume; **D** - dimensional, **d** - atmospheric precipitation; **dep** - dry deposition; **diag** - diagnostic; **doubstoch** - doubly stochastic; **dust** - dust; **emi** - emission data; **Eul** - Eulerian; **exp.rep** -expert's report; **f** - relative humidity; **field** - field experiment mesurements; γ - Pasquill classification; τ_d - deposition time; **Gaus** - Gaussian; **grid** - grid, numerical; **H** - mixing layer height; **hemet** - heavy metals; **imi** - imission data; **k** - chemical transformation rate; **Kalm** - Kalman filter; λ - scavenging ratio; **lay** - layers; **line** - line; **local** -local; **Lgr** - Lagrangian; **N** - cloud cover; **othem** - others meteorological parameters; **othes** - others sources parameters; **othin** - other input data; **oper** - operating; **p** - atmospheric pressure; **pars** - source parameters; **point** - point; **prepr** - from preprocessor; **prog** - forecasting, prognostic; **Psq** - Pasquill; **rad** - radioactivity; **radde** - radioactive decay; **rad-dust** - radioactive dust; **reas** - researching; **reg** - regional; s_o - concentration background of pollutions; **segpl** - segmented plume; **soil** - soil thermal and wetness parameters; **spect** - spectral; **stand** - standard measurements; **stat** - statistical; **T** - temperature; **top** - topography, **wash** - washout; **veg** - vegetation cover; **v** - wind; v_d - dry deposition velocity; **volum** - volume; z_o - surface roughness coefficient; **[-]** - no information;

Numerous models applied in engineering practice use otherwise known regressive models, such as multiple regression and time series analysis. ARIMA — the Auto Regressive Integrated Moving Average is a model in which concentration forecast at a fixed point or mean for an area is expressed as a linear combination of concentrations in the past period and a purely random term (white noise). ARX-*A*uto *R*egressive with e*X*ogeneous input is an ARIMA model with an external input *(Morawska-Horawska* and *Tumidajski*, 1988). Pollution concentration in a given time interval is expressed here by a linear combination of past concentrations and external meteorological parameter values plus a random term. This model use is justified solely in climates with high weather pattern persistency, since synoptic and seasonal atmospheric variability cannot be avoided.

3. Model input data

The sets of input data for dispersion models may be divided into four groups:

- modeled area parameters defining characteristic features of the modeled area (roughness, vegetation, hypsometry, soils). These are prerequisite to numerical models; in analytical models, surface is usually defined solely by the roughness parameter,
- parameters defining the emission source — most often very difficult to obtain,
- parameters defining chemical changes occurring in pollution in the atmosphere — they are usually insufficiently identified. A complete description of pollution chemistry in the model should comprise about 1,000 reactions occurring between hundreds of various substances. Constant values defining the rate of reactions depend on numerous factors, i.e.: season of the year, part of the day, air humidity, presence of other substances which may act as catalysts,
- meteorological data.

The complex structure of a dispersion model accounting for a wide range of physical processes occurring in the atmosphere as well as chemical and/or nuclear changes requires information about meteorological variables, their spatial fields and transformations in time. Such data may be obtained from the so-called meteorological preprocessors only. These are primarily meteorological numerical models in macro or regional scale, operating in national or continental centers. Such a preprocessor may also be constituted by a numerical model of the atmospheric boundary layer on local, meso or regional scale, which generates a set of meteorological data exclusively for a specific diffusion model. Preprocessors are also the simple integral models of the mixing layer developed in Denmark (*Sorbjan,* 1989) and the uncomplicated models using the

similarity theory of the surface layer or boundary layer. Numerous models use standard data from meteorological synoptic stations; however they mainly include wind measurements at 10 m altitude, temperature measurements at 2 m altitude and cloud cover. Meteorological measurement data introduced into dispersion models should be *representative* of the modeling area with respect to the adopted averaging period (*Pruchnicki*, 1987). Current or historical measurement data should be controled and assimilated in accordance with the currently adopted techniques. Meteorological data processing may include interpolation to grid nodes. In case of winds for scales other than local a diagnostic model is required, satisfying the continuaity equation. The computation of Pasquill equilibrium classes is also included into the processing. Pollution emission measurements belong to the model input data set. These primarily come from monitoring networks and other gauge stations, registering pollution concentrations systematically at fixed times or automatically on a continuous basis.

4. Model evaluation problem

Authors of models developed in Poland only in a few cases provide information about verification against measurement data. A field experiment was organized in Cracow MONAT'84 *(Nowicki*, 1985) for models URFOR2, MOD and SPM. Dispersion models LPD and EGD, incorporated into the atmospheric mesoscale dispersion modeling system MDMS (*Uliasz*, 1993) package were verified against the mesoscale meteorological and dispersion experiment organized over Øresund strait on Baltic Sea. The Kalman filter model *(Twardowska,* 1989) was verified in Uppsala Silesia Industrial District against monitoring data TEST-88.

The model evaluation problem is too extensive to be discussed in this review, we shall just list the sources and types of modeling uncertainties. Difficulties in the mathematical definition of the atmospheric processes as well as measurement problems are the main reasons of model inadequacies. The atmosphere is highly variable in time and space, hence the models should be verified against measurement data in various weather conditions. Insufficient identification of chemical reactions affecting pollution in the atmosphere may have an essential impact on modeling outputs. Even the best diffusion model with high class meteorological preprocessor shall fail to provide results in line with the measurements if we overlook the natural decomposition of pollution or creation of a given compound in the atmosphere in various circumstances outside the emission source.

Uncertainty of modeling dispersion in the atmosphere (*Venkatram*, 1988) primarily results from the stochastic structure of atmospheric turbulence, but it is also related to the possibility of the comparison of results obtained in various models. This is linked with the notion of averaging over ensemble and with

random process realization. *Inherent* relates to the mean deviation between the concentration measured during one (of many) realization and the concentration averaged over the ensemble. The main problem resides in that the definition of 'ensemble' is not precise enough against real measurements. Modeling uncertainty also comprises errors in input data, errors in formulating the ensemble average (these are systematic errors): Model uncertainty analysis may to a certain extent become its means of evaluation.

Recapitulating, we can say that numerous dispersion models have been developed in Poland; modeling methods and levels are highly diverse. The majority of models were neither verified nor evaluated in terms of modeling outputs. The position of Poland in this field is noticeable. Many of the herein presented models are of high international standard, some of theme are unique *(Kazimerczyk et al.,* 1993).

Anna Madany asks the inquiry respondents for forgiveness: limited space in Időjárás publication did not allow the presentation of all the 84 publications of Polish model developers nor more extensive information about them, comprised in the article published in Polish by Madany and Bartochowska (1995).

References

[1] Abert, K., Budziński, K. and *Juda-Rezler, K.*, 1994: Regional air pollution models for Poland. *Ecological Engineering, Elsevier Science Publishers 3,* 225-244.

[2] *Bartnicki, J.*, 1994: Tree-dimensional long-range pseudospectral model for atmospheric transport of sulphur oxides. *Tech. Desc. Report of MSC-E*, Moscow.

[3] *Cibor, R., Rymarz, Cz.* and *Woźniak, M.*, 1984: Algorithm for computing local transport of chemical compounds with consideration for meteorological conditions. *Bull. MUT. XXX*, Warsaw (in Polish).

[4] *Chróściel, St. et al.*, 1984: Development of a computer software for REGSIM model. *Report PR8*, No. 7.2.3.3.b2, WUT Warsaw (in Polish).

[5] *Chróściel, St.* and *Markiewicz, M.*, 1985: Modeling of the atmospheric dispersion of sulphur dioxide in the urban Cracow agglomeration. *Envir. Prot. Engin.*, Vol. II, 65-72.

[6] *Dąbrowski, D.*, 1991: Assessment of radiological contamination model for nuclear power station. *Report Central Laboratory of Radiation Protection*. Warsaw (in Polish).

[7] *Hrehoruk, J. et al.*, 1993: Regional heavy metals of atmospheric transport model for Poland. *Reports of IMWM 3,* (in Polish).

[8] *Haman, K.E.* and *Malinowski, S.P.*, 1989: Observations of stack and cooling tower plumes and their comparison with plume model ALINA. *Atmos. Environ. 23*, 1223-1234.

[9] *Holnicki, P. et al.*, 1993: A multilayer computer model for air quality forecasting in urban/regional scale. *Control and Cybernetic 22,* No. 3, 5-28.

[10] *Jagusiewicz, A.*, 1980: *Methodics of Atmospheric Air Pollution Long-Term Forecasting*. Ed.: Environment Cultivation Institute, Warsaw (in Polish).

[11] *Juda-Rezler, K.*, 1986: Modelling of the air pollution in the Cracow area. *Atmos. Environ. 20,* 2449-2558.

[12] *Juda-Rezler, K.*, 1991: *Classification and Characteristics of Air Pollution Models Chemistry for Protection of the Environment*. Plenum Publishing Corporation, New York.

[13] *Juda-Rezler, K. et al.*, 1996: *Emission Abatement Strategies and the Environment Progress Report*. Copernicus, Warsaw University of Technology.

[14] *Kazimierczyk, P., Szabłowski, P.J.* and *Twardowska, K.*, 1993: Estimation and prediction of pollutant concentrations involved in nitrogen oxides cycles a doubly stochastic model. *Appl. Math. and Compt. Sci. 3,* 731-750.

[15] *Madany, A. et al.*, 1995: Numerical modeling of air pollution transport in Central Europe and preprocessing of meteorological data. *Proc. of Polish-British Conference.* Environmental Engineering, Warsaw, 16-18 Oct 1995, 142-148.

[16] *Madany, A.* and *Bartochowska, M.*, 1995: Review of Polish air pollution dispersion models. *Sc. Papers Warsaw Univ. of Technology 19*, 73-110 (in Polish).

[17] *Markiewicz, M.*, 1994: The Gaussian air pollution dispersion model with variabiliy of input parameters taken into account. Part I, II. *Envir. Prot. Engineering 1-4.*

[18] *Morawska-Horawska, M.* and *Tumidajski, T.*, 1988: Statistical models of mean daily SO_2 concentration in Cracow. *Reports of IMWM, Vol. IX,* No. 3 (in Polish).

[19] *Nowicki, M.*, 1985: MONAT 84, Experimental study for the needs of air pollution control in Cracow, Poland. *Environ. Protect Eng. 11*, No. 2, 11-15.

[20] *Pruchnicki, J.*, 1987: Methods of climatological data elaboration. *Polish Sc. Public.*, Warsaw, 203 (in Polish).

[21] *Sorbjan, Z.*, 1989: *Structure of the Atmospheric Boundary Layer.* Prentice Hall.

[22] *Szepesi, D.J.*, 1989: *Compendium of Regulatory Air Quality Simulation Models.* Akadémiai Kiadó, Budapest.

[23] *Twardowska, K.*, 1989: The stochastic processes and filtering theory in the prediction of air pollution in the Silesian district. *Proc. of the 28th SICE Annual Conference*, Vol. II., July 25–27, 1989 Matsuyama.

[24] *Uliasz, M.*, 1990: Development of the mesoscale dispersion modeling system using personal computers. Part I: Models and computer implementation. *Z. Meteor. 40,* 104-114, Part II, 285-298.

[25] *Uliasz, M.*, 1993: The atmospheric mesoscale dispersion modeling system. *J. Appl. Meteor. 32*, 139-149.

[26] *Venkatram, A.* 1988: Inherent uncertainty in air quality modeling. *Atmos. Environ. 22*, 1211-1227.

[27] *Venkatram, A.* and *Seigneur, Ch.*, 1993: Review of mathematical models for health risk assessment: II Atmospheric chemical concentrations. *Envir. Software 8*, 75-99.

[28] *Winnicki, J.*, 1989: Air pollution dispersion model in the atmospheric boundary layer. *Report 02/072/WAT.KOAS.* Military University of Technology, Warsaw (in Polish).

[29] *Winnicki, J.*, 1990: Theoretical basis for development of a pollution dispersion model in the atmospheric surface layer with orography in generalised Philips coordinates. *Report 01 KOAS.* Military University of Technology, Warsaw (in Polish).

IDŐJÁRÁS

Quarterly Journal of the Hungarian Meteorological Service
Vol. 101, No. 1, January–March 1997, pp. 45–54

Influence of the foundry plant operation on the heavy metal level in the air of New Belgrade in the reduced production regime

Dragana Đorđević[1], **Dušan Jovanović**[2], **Zorka Vukmirović**[3] and **Dragan Veselinović**[4]

[1]*Holding Co., Workers Safety, Fire and Environmental Protection, Deskaševa 7, YU-11000 Belgrade, Yugoslavia*
[2]*IChTM-Institute of Catalysis and Chemical Engineering, Njegoševa 12, YU-11000 Belgrade, Yugoslavia; E-mail: dusanmj@hf01.chem.bg.ac.yu*
[3]*Institute of Physics, Pregrevica 118, YU-11080 Zemun, Yugoslavia*
[4]*Faculty of Physical Chemistry, Studentski trg 12-14, YU-11000 Belgrade, Yugoslavia*

(Manuscript received 13 November 1995; in final form 19 February 1996)

Abstract—Due to their extensively deteriorating influence on biosphere, heavy metals in the human environment have been intensively monitored during the recent years. From September 1992 to September 1993, we continually monitored the content of heavy metals in the air of the New Belgrade industrial zone. We proved that the operation of the foundry BCF (Belgrade Casting Factory) influenced the heavy metal content in the air of its surroundings. BCF is an industrial complex located within an urban, densely populated area of New Belgrade. It has also been recorded that other sources were influencing the heavy metal content in the air, primarily the local wind re-suspension of soil particles, wind-transport from distant locations, etc.

Key-words: human environment, heavy metal monitoring, wind re-suspension.

1. Introduction

Heavy metals are emitted into the environment due to various human activities. They are widely used in industry and in the course of the smelting and combustion processes they are emitted mainly to the atmosphere. The main emission sources are:

- metal-processing industry,
- energy production, and
- road traffic.

Heavy metals are significant for their contribution to air pollution. In recent years their presence has been monitored all over Europe. From them As, Be,

Cd, Co, Cr, Cu, Hg, Mn, Ni, Pb, Sb, V, Zn, Se and Zr are of particular interest. The above mentioned metals' negative influence on the biosphere attracts an increased attention of researchers (*Guthner*, 1989; *Kurfurst*, 1989; *Santroch*, 1989). From September 1992 to December 1995 the economic sanctions influenced the production level and the continuity of the New Belgrade foundry plant operation. That enabled us to monitor the content of some heavy metals in the air in the conditions of the reduced production, as well as during the operation shut-downs, including the influence of the previous soil-pollution on the pollution during the mentioned period of time.

2. Database

2.1 Sampling site and period

This study has been aimed at the investigation of the heavy metal content in the air surrounding the foundry plant as influenced by its operation. The testing was made at five measuring spots that were located from 100 to 400 meters from the emission source, in different directions (as shown in *Fig. 1*) and positioned in a manner that enabled the monitoring of the heavy metal spreading.

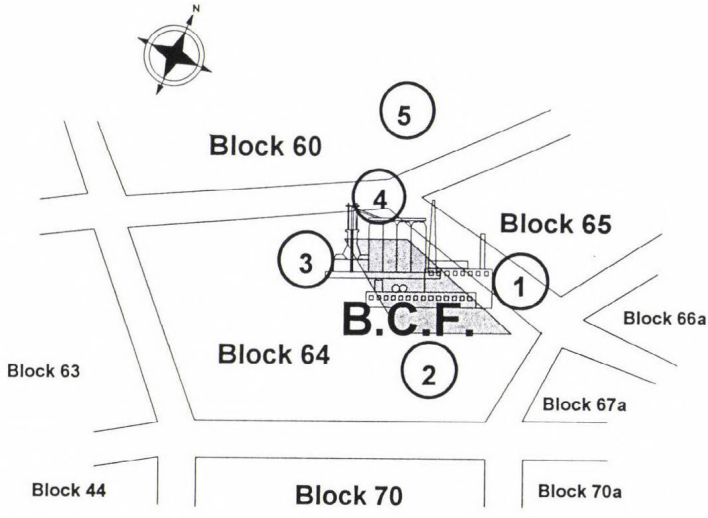

Fig. 1. Position of the Belgrade Casting Factory (BCF) with the positions of the measuring spots (1–5) as marked.

The Belgrade Casting Factory — BCF (Fabrika odlivaka Beograd — FOB) in New Belgrade was built in 1947 and the new foundry plant became

operational in 1977. It is located at the territory of the residential Block 64 (New Belgrade). It is a unique example of a newly constructed foundry plant within a residential area (Fig. 1). The foundry is located at the City of Belgrade territorial grounds (at the geographic latitude of 44°48'20''N and the geographic longitude of 20°25'30''E).

To the west of BCF there is the metalworking industrial complex (IMT) and to the southeast there is the Central City Heating Plant; one closer and the other further, respectively. Around the mentioned plants and between the residential blocks there are heavy-traffic arteries.

The basic source of the metal pollution in a smelting process is the furnace. The complexity of the technological process in a foundry is increased by a large number — more than 50 — of basic raw materials. The material is smelted and homogenized, and it leaves the furnace at the temperature of 1520°C–1550°C. The smelting process causes the rise and separation of different gases and waste materials.

The capacity of the foundry is about 1,000 tons of castings a month. In the last few years, i.e. from 1988 on, the production level was about 3,500 tons/month, with a drop in 1991 but with no interruptions. All the way through December 1992, the foundry continued to operate, although with a further drop of the production level, and then it shut down its operation. At the end of March 1993 the furnaces were started again and the reduced production process continued all through August 1993, the next shut-down. *Fig. 2* presents the production level in the period from September 1992 to September 1993.

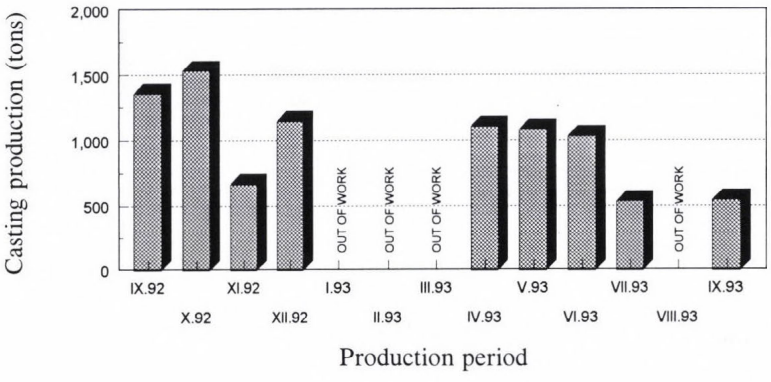

Fig. 2. Belgrade Casting Factory production level: September 1992–September 1993.

From September 1992 to September 1993, the samples were taken at the five designated (and mentioned) measuring spots, and in April 1993 an

additional measuring spot (measuring spot No. 6) was introduced. It is located within the eco-meteorological station at Ušće — New Belgrade.

At the onset of our investigations we monitored the Fe, Cu, Ni, Pb, Cd and Cr concentrations in the air surrounding the foundry complex, and since April 1993, in addition to the above mentioned metals, the concentrations of Mn, Zn and As were monitored as well.

2.2. The sample-taking process

The sampling system consists of a controlled-flow (app. 1 dm^3/min) membranous pump, a membranous PTFE filter of 1.0 μm and 0.22 μm pore openings, a gas meter and a probe mounted at 1.5 m above the ground with its opening facing downwards. In these conditions, and in a no-wind situation, we performed sampling of the particles of a diameter <20.0 μm (*Katz*, 1977; *Marendić-Miljković et al.*, 1989). The analysis of the investigated metals was done by the method of Atomic Absorption Spectrometry (AAS) using the VARIAN SpectrAA-20 Plus device. The standardizing of a solution for AAS analysis was performed through a precise measuring-up of the previously dried-up salt (at 105°C to constant mass) of the corresponding metal and by its diluting in the HNO_3/HCl solution in a normal dish. The arsenic was determined by a so-called hydride technique. The skimming of deposits off the membranous filter was done through a quantitative diluting in the HNO_3/HCl mixture, after which the solution was analyzed on AAS referred to as the 'blank' test. The standard AAS solutions were made by the usual analytical technique with adequate diluting. A calibration curve in the optimal measuring range was made for each individual metal.

3. Results and discussion

The average concentration data for Fall 1992, Winter 1992/93, Spring 1993 and Summer 1993, for each element (ng/m^3) and measuring position spot (Pos. 1.–Pos. 5), with the corresponding wind rose, are presented in the tables below (*Table 1–Table 4*).

The data clearly show that the copper concentrations, used for computing the average seasonal concentrations in summer, are below the detection limit for the given sampling conditions. Also, the average nickel and chromium concentrations in summer are below the detection margin for the given sampling conditions, while the average manganese concentrations are within the instrument's detection range for the given sampling conditions.

There are no reliable conclusions for the copper, nickel, chrome and manganese concentrations in spring and summer.

Table 1. Average concentrations (ng/m^3) and the wind rose for Fall 1992

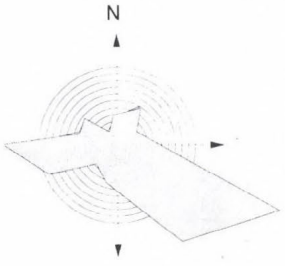

	Pos. 1	*Pos. 2*	*Pos. 3*	*Pos. 4*	*Pos. 5*
Cd	55	35	-	66	45
Cr	1400	360	50	900	550
Cu	78	82	140	157	79
Fe	460	280	-	410	230
Ni	110	240	-	500	450
Pb	490	430	940	760	640

Table 2. Average concentrations (ng/m^3) and the wind rose for Winter 1992/1993

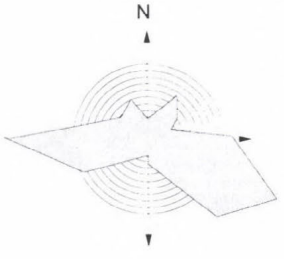

	Pos. 1	*Pos. 2*	*Pos. 3*	*Pos. 4*	*Pos. 5*
Cd	24	18	10	43	21
Cr	70	50	50	80	60
Cu	24	50	18	60	28
Fe	330	160	320	240	150
Ni	70	60	60	120	70
Pb	160	100	110	190	120

Table 3. Average concentrations (ng/m^3) and the wind rose for Spring 1993
(dl – detection limit)

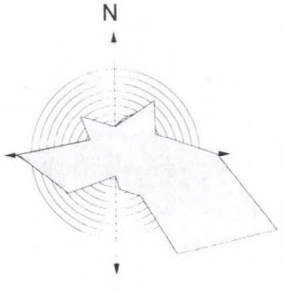

	Pos. 1	*Pos. 2*	*Pos. 3*	*Pos. 4*	*Pos. 5*
Cd	16	10	10	20	10
Cr	220	210	500	390	190
Cu	< dl	< dl	< dl	10	< dl
Fe	550	350	680	560	450
Ni	< dl	< dl	< dl	< dl	< dl
Pb	160	120	130	200	100
As	90	118	336	87	98
Mn	60	60	30	140	30
Zn	55	89	56	225	62

Table 4. Average concentrations (ng/m^3) and the wind rose for Summer 1993 (dl – detection limit)

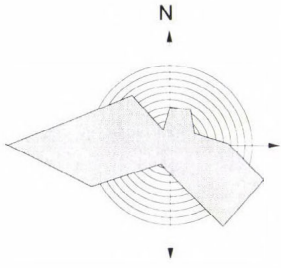

	Pos. 1	*Pos. 2*	*Pos. 3*	*Pos. 4*	*Pos. 5*
Cd	24	16	68	24	15
Cr	< dl	< dl	< dl	< dl	< dl
Cu	< dl	< dl	< dl	< dl	< dl
Fe	200	80	300	170	170
Ni	< dl	< dl	< dl	< dl	< dl
Pb	150	100	370	200	150
As	8	18	13	12	12
Mn	40	30	20	20	20
Zn	32	20	44	15	26

It is interesting to compare the measurements obtained in Milan, Vienna, Budapest and the regional K-puszta station (which is about 100 km southeast off Budapest, Hungary) with the concentration values (see *Table 5*) (*Molnár et al.*, 1993).

Table 5. Six-month (July-December 1991) average concentrations of metals in the air of the urban zones of the surrounding countries and the regional K-puszta station, in ng/m^3

	Milan	K-puszta	Budapest	Vienna
Cu	100.0	4.4	20.0	22.0
Cr	10.0	4.8	9.8	6.5
As	20.0	3.7	22.0	-
Zn	800.0	21.8	136.0	50.0
Mn	9.1	3.4	13.0	19.0
Ni	10.0	1.9	6.1	11.0
Fe	5,000.0	194.0	715.0	520.0
Pb	500.0	10.4	203.0	83.0

It is interesting to note that the individual elements' concentrations (Fe, Pb, As, Mn and Zn) taken in the industrial part of New Belgrade, where the metal-processing industry is located, in spring and summer, are close to the ones taken in Milan, Budapest and Vienna. The Zn concentrations in summer are close to those measured at the regional K-puszta station in Hungary which is far away from any urban zone.

The economic sanctions introduced in June 1992 caused the reduction of both the industrial production and the highway traffic frequency (due to the motor vehicle gas import embargo). The effect of the sanctions was the most

severe in spring and summer 1993. It caused the shut-down of almost all industrial facilities and reduced the traffic to a minimum. One of the consequences was a drop of the heavy metal concentration in the air of the New Belgrade industrial zone. In the course of the sampling BCF operated at about 15% of its capacity and with occasional shut-downs. Such conditions did not enable the monitoring of the factory's influence on the heavy metals in the air, since there were other sources that probably contributed to it; local wind re-suspension, primarily; aerosol transport from the highly contaminated distant locations; mechanical re-suspension, as well as the trash incineration (the probable source of Cr and As contained in the dyes).

The heavy metal content in the air in the measuring period was most probably very highly influenced by the local wind re-suspension of the particles that precipitated into the soil due to the foundry plant operation in the course of the years.

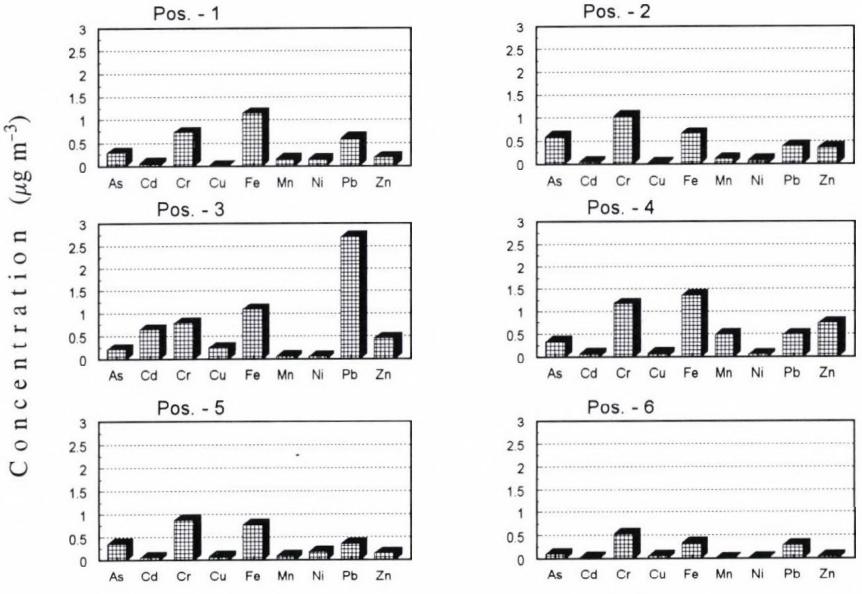

Fig. 3. Histograms of the maximal element concentrations measured at all the measuring positions including the position spot No. 6 (Ušće), for the period from April 1993–September 1993.

The histograms (*Fig. 3*) show that the maximal concentrations measured around the plant are considerably higher that those measured at Ušće. In the conditions of the significantly low operation regime (throughout the measuring

period), no significant differences were to be expected as Ušće is quite far (about 3,000 m) from the monitored emission source, and because the sampling included particles with long atmospheric residence time that were easily transported to large distances. Upon analyzing these values and having in mind that the production regime was very low and that the measuring spot No. 6 (Ušće) is above the grass, where the re-suspension effect is negligible, it is possible to claim that the re-suspension process is dominant in the vicinity of the plant. This conclusion is supported by the results obtained by averaging the concentration of the investigated metals over the period when the foundry did not work (January–March 1993 and August 1993), as shown in *Tables 6* and *7*.

Table 6. Average metal concentration values in the air around the foundry from January to March 1993

	Pos. 1	Pos. 2	Pos. 3	Pos. 4	Pos. 5
Cd	21	16	10	38	18
Cr	80	60	370	210	110
Cu	<5	<5	<5	20	<5
Fe	2160	160	510	290	180
Ni	40	40	20	70	40
Pb	130	60	130	120	60

Table 7. Average metal concentration values in the air around the BCF plant in August 1993 (dl – detection limit)

	Pos. 1	Pos. 2	Pos. 3	Pos. 4	Pos. 5
Cd	52	24	15	43	28
Cr	<dl	<dl	<dl	<dl	<dl
Cu	<dl	<dl	<dl	<dl	<dl
Fe	200	60	210	200	110
Ni	<dl	<dl	<dl	<dl	<dl
Pb	140	50	80	130	50

After reviewing the series of individual data and choosing the statistical distribution functions that describe the influence of the emission source, we tried to define the empirical functions through theoretical functions. Two theoretical functions were chosen: log-normal, best describing the influence of a constant emission source, and Weibull's theory that is best for describing the wind re-suspension. The Kolmogorov-test was used for fitting the empirical distributions with the theoretical functions. This analysis did not yield a good

match, which implies that the problem is complex due to the influence of a larger number of various processes on the heavy metal content in the air. Only the series of data pertaining to iron gives a proximate match with the theoretical function of the log-normal distribution, which implies that for this element the Casting Plant (BCF) is indeed a dominant emission source (*Garger et al.*, 1994; *Vukmirović*, 1989). The mis-match of the empirical and theoretical functions is indicative of the existence of a large number of equally dominant emission sources, except for iron. This is due to the fact that the added metal content in a casting charge is changed in dependence of the quality requirements, while the percentage of iron is fairly constant.

The Hydrometeorological Institute of the Republic of Serbia provided us with wind roses (seasonal and annual) for the period September 1992–September 1993 from the Surčin Meteorological Station, which is most representative for the New Belgrade territory. For this territory, the dominant wind courses are from the east and west-southwest direction, marked as prolonged acute angles of the polygons in such directions. The wind data were necessary to define the correlation between the dominant wind courses and the metals' concentration level in those directions. The measuring spot No. 3 was located to the east and the measuring spot No. 1 was located to the west-southwest. It has been found that the iron follows this correlation in winter, spring and summer, while the cadmium follows it in summer only. The other elements do not follow the dominant wind courses.

4. Conclusion

In the second measuring period the sampling conditions were unfavorable for defining the level of copper, nickel, chrome and manganese. High concentrations in the first measuring period (Fall–Winter) could be explained by their high concentrations in the particles originating from the wind re-suspension. With the foundry shut-down, in the course of time and especially after the seasonal rainfalls, these metals have been diluted, washed-down and migrated into the soil, which, in turn, reduced their level in the re-suspended particles.

In addition to the Casting Plant (BCP), there are other sources of heavy metal emission into the air, from which the most probable one is the re-suspension off the soil, except for iron for which the casting plant is a dominant source.

During that period the heavy metal concentration in the air did not drastically differ from the concentrations of the neighboring countries' urban zone air, with the Zn concentrations being in the order of magnitude of the ones measured at the regional K-puszta station.

The results of this study are significant for the environment restoration strategy, since they indicate that the metals are present around the industrial sources even after a drastic reduction in their emission.

References

Garger, E., Kashpur, V., Gurgula, B., Paretzke, H. and *Tschiersch, J.*, 1994: Statistical characteristics of the activity concentration in the surface layer of the atmosphere in the 30 km zone of Chernobyl. *J. Aerosol Sci. 25*, 767-777.

Guthner, G., 1989: Remarks on control of heavy metal emission in the Federal Republic of Germany. First Meeting 'Heavy Metal Emissions', Vol. 1, Prague, 24-26 Oct 1989.

Katz, M., 1977: *Methods of Air Sam-pling and Analysis*. APHA, Washington.

Kurfurst, J., 1989: ECE Project 'Heavy Metals Emissions', First Meeting 'Heavy Metal Emissions', Vol. 1, Prague, 24-26 Oct 1989.

Marendić-Miljković, J., Marković, D., Vukelić N. and *Vukmirović, Z.*, 1989: Trace metal deposition in the complex orographic conditions. *Proc. XIV International Conference on Carpathian Meteorology*, Sofia, 25-30 Sep 1989.

Molnár, Á., Mészáros, E., Bozó, L., Borbély-Kiss, I., Koltay, E. and *Szabó, Gy.*, 1993: Elemental composition of atmospheric aerosol particles under different conditions in Hungary. *Atmos. Environ. Part A, 27A*, 2457-2461.

Santroch, J., 1989: Heavy metals in atmospheric aerosol and deposition. First Meeting 'Heavy Metal Emissions', Vol. 1, Prague, 24-26 Oct 1989.

Vukmirović, Z., 1989: Lognormal distribution application for air-quality assessment. *J. Serb. Chem. Soc. 54*, 373-381.

IDŐJÁRÁS

Quarterly Journal of the Hungarian Meteorological Service
Vol. 101, No. 1, January–March 1997, pp. 55–64

Characteristic global and diffuse solar radiation values for Serbia

Miroslava Unkašević

Faculty of Physics, Institute of Meteorology, University of Belgrade,
11001 Belgrade, P.O. Box 550, Yugoslavia
E-mail: itosic@rudjer.ff.bg.ac.yu

(Manuscript received 13 November 1995; in final form 19 February 1996)

Abstract—Monthly mean global and diffuse solar radiation values recorded by the radiation network of the Serbian Meteorological Service were analyzed in order to derive characteristic elements of the solar climate from seven typical Serbian locations. The diffuse solar radiation was estimated for the stations where such data were not available by means of formulae relating the measured data to the 'clearness index' K, which is expressed as a function of the global and extraterrestrial solar radiation, and to the sunshine index I, which depends on the sunshine ratio n/N, where n is the monthly mean daily value of bright sunshine hours and N is the maximum possible value of sunshine hours. The relationship between the diffuse and global radiation leads to the conclusion that the 'clearness index' does not adequately describe all the climate variables. It can be stated that individual formulae based on the direct regression analysis of the measured data are necessary for different climatic and geographic areas.

Key-words: global and diffuse radiation, 'clearness' and sunshine indexes, correlation.

1. Introduction

The only available data of solar radiation from a number of locations are measurements of global radiation on a horizontal surface. Diffuse solar radiation data, which are necessary to design solar energy collecting systems, are usually not available.

Many studies dealing with the global solar radiation at various locations and regions of Southern Europe were made in the past (e.g. *Elena et al.*, 1981; *Pasquale*, 1987; *Santamouris* and *Katsoulis*, 1989; *Katsoulis et al.*, 1991), whereas *Katsoulis* (1991) has carried out a comparison of several diffuse solar radiation models for Greece.

The purpose of the present work is to investigate the solar radiation in Serbia and to test the applicability of a correlation model for the estimation of diffuse radiation at one site, Belgrade-Zeleno Brdo (φ = 44°47'N, λ = 20°23'E, h = 243 m asl). Only two stations in Serbia have relatively long-term records of global and diffuse radiation (Belgrade-Zeleno Brdo and Sjenica), whereas five stations can measure only the global radiation on the horizontal plane. Therefore, an estimate of the ratio of diffuse to global radiation would increase the usefulness of the existing data. There are several statistically-based correlation models relating global radiation G and its diffuse component D. The models accepted for estimating the horizontal diffuse solar radiation are of two types (*Lewis*, 1987). The first type is based on the expression of the monthly mean daily diffuse radiation ratio, D/G, as a function of the monthly mean daily 'clearness index' $K = G/G_0$ (G_0 is the extraterrestrial solar radiation). The second type, which is applied here as it correlates better with the measured values, is based on the expression of the ratio D/G or D/G_0 as a function of the sunshine index I (*Pasquale*, 1987), which is defined by the monthly mean daily value of bright sunshine hours, n, and the maximum possible sunshine N.

2. *Analysis of global solar radiation*

The measurements of global and diffuse solar radiation in Serbia began during the 1957–1958 International Geophysical Year. The network consisted of seven radiation measuring stations (*Fig. 1*), whose geographical coordinates and recording periods are shown in *Table 1*. Four stations are located in urban areas (Novi Sad, Belgrade-Zeleno Brdo, Negotin and Priština), whereas three are located on high mountains (Sjenica, Zlatibor and Kopaonik). The global solar radiation is measured by Moll-Gorczynski pyranometers, while the diffuse radiation is measured by diffusographs consisting of the above pyranometers equipped with special shading devices whose purpose is to exclude the direct radiation from the sun.

The monthly mean values of the global radiation available on horizontal surfaces for each station are listed in *Table 2*. These values have been derived from the daily totals of each month of the periods shown in Table 1.

Although the periods of observation are not the same in all the stations, some general conclusions may be drawn from the data. Although the local effects may be considerable, the data of global solar radiation are related to the geographic latitude. In the urban areas G has maximum values in June–July, (22.04–23.83 MJ m^{-2} day^{-1}) and minimum values in December (3.31–4.85 MJ m^{-2} day^{-1}). The mountain stations, because of their high elevation, show in the colder part of the year higher global radiation. Here the maximum of G (21.44–22.26 MJ m^{-2} day^{-1}) is recorded in July, whereas the minimum (4.80–5.62 MJ m^{-2} day^{-1}) is again in December.

Fig. 1. Territory of Serbia (full circles showing recording network for solar radiation). The insert in the upper right-hand corner shows the region relative to the remaining parts of former Yugoslavia and surrounding countries.

The data from Belgrade-Zeleno Brdo and Negotin stations (similar geographical latitude) can be taken as an example of the local effects on the global radiation. Negotin receives in the colder part of the year a smaller amount of global radiation than Belgrade-Zeleno Brdo, whereas the global radiation is higher in the warmer part of the year. Negotin is located behind mount Deli Jovan, near river Danube, so that fogs are frequent during the colder part of the year, while the Belgrade-Zeleno Brdo station is located out of the town centre.

3. Analysis of diffuse solar radiation

In order to calculate the diffuse component of the global radiation on a monthly basis on a horizontal surface at stations where actual diffuse radiation data are not available (Novi Sad, Negotin, Kopaonik, Zlatibor and Priština), we have worked out an equation relating the D/G ratio to the 'clearness' parameter K, based on long-term data from the Belgrade-Zeleno Brdo station. Relevant meteorological and solar radiation data for Belgrade-Zeleno Brdo and Sjenica are given in *Tables 3* and *4*. Because of its high elevation and lower geographical latitude Sjenica receives during the year a higher diffuse radiation than Belgrade-Zeleno Brdo.

Table 1. Geographic coordinates of the stations and recording periods

No.	Station	Period	Measurement
1.	*Novi Sad* φ = 45°20'N λ = 19°51'E h = 84 m asl	1964–1986	global
2.	*Belgrade-Zeleno Brdo* φ = 44°47'N λ = 20°23'E h = 243 m asl	1957–1990	global, diffuse
3.	*Negotin* φ = 44°14'N λ = 22°33'E h = 42 m asl	1957–1990	global
4.	*Zlatibor* φ = 43°44'N λ = 19°43'E h = 1029 m asl	1957–1986	global
5.	*Kopaonik* φ = 43°17'N λ = 20°48'E h = 1711 m asl	1981–1990	global
6.	*Sjenica* φ = 43°16'N λ = 20°01'E h = 1015 m asl	1964–1974	global, diffuse
7.	*Priština* φ = 42°39'N λ = 21°09'E h = 573 m asl	1967–1990	global

Table 2. Global solar radiation data for stations in Serbia (MJ m^{-2} day^{-1})

Station	Jan	Feb	Mar	Apr	May	Jun	Jul	Aug	Sep	Oct	Nov	Dec
Novi Sad	4.89	7.58	11.72	16.01	19.74	22.09	22.02	19.18	14.37	9.88	5.11	3.31
Belgrade	5.22	7.90	12.68	16.56	20.17	22.37	22.29	19.93	15.36	10.52	5.73	3.77
Negotin	4.76	7.53	11.59	15.97	21.05	23.25	23.83	20.89	15.87	10.95	4.75	3.59
Zlatibor	5.83	8.68	12.20	15.70	18.63	20.88	21.44	19.23	14.90	10.50	6.28	4.80
Kopaonk	6.80	10.02	13.22	16.63	19.70	21.82	22.26	19.50	14.99	10.87	6.61	5.38
Sjenica	6.91	10.21	14.28	17.01	20.44	22.74	22.84	20.18	19.85	11.36	7.57	5.62
Priština	5.88	8.69	13.53	16.96	20.24	22.43	22.18	20.45	15.65	11.52	6.78	4.85

Table 3. Indexes *K* and *I* and measured and estimated values of diffuse solar radiation for Belgrade-Zeleno Brdo

Month	K	I	D′ measured (MJ m^{-2} day^{-1})	D′ estimated from equations (MJ m^{-2} day^{-1}) for Belgrade-Zeleno Brdo					
				(1)	(2)	(3)	(4)	(5,6,7)	(8)
Jan	0.42	0.25	3.16	2.99	2.74	2.32	2.99	4.75	3.00
Feb	0.44	0.33	4.68	4.18	3.95	3.53	4.34	6.75	4.45
Mar	0.49	0.41	6.16	5.91	5.59	4.82	6.21	9.84	6.40
Apr	0.50	0.47	8.23	7.58	7.28	6.14	8.01	12.50	8.25
May	0.51	0.50	9.34	9.09	8.46	7.32	9.32	14.70	9.35
Jun	0.54	0.55	9.95	9.80	8.82	7.61	9.72	15.56	9.51
Jul	0.55	0.63	9.17	9.73	8.41	7.38	9.00	14.67	8.26
Aug	0.56	0.64	7.99	8.70	7.32	6.44	7.87	13.28	7.14
Sep	0.54	0.58	6.40	6.73	6.03	5.22	6.55	10.46	6.28
Oct	0.51	0.49	4.62	4.74	4.45	3.82	4.91	7.73	4.94
Nov	0.41	0.31	3.24	3.34	3.07	2.61	3.38	5.15	3.46
Dec	0.35	0.24	2.52	2.75	2.30	1.98	2.61	3.82	2.61
RMSE				0.397	0.662	1.487	0.197	3.969	0.282

Table 4. Index *I* and measured and estimated values of diffuse solar radiation data for Sjenica

Month	I	D′ measured (MJ m^{-2} day^{-1})	D′ estimated from Eq. (8) (MJ m^{-2} day^{-1})
Jan	0.27	4.82	4.28
Feb	0.32	6.47	6.00
Mar	0.39	7.68	7.77
Apr	0.43	8.80	8.81
May	0.46	9.88	10.20
Jun	0.49	10.72	10.92
Jul	0.51	10.58	10.64
Aug	0.50	8.80	9.55
Sep	0.49	7.14	7.61
Oct	0.48	4.87	5.52
Nov	0.41	3.81	4.02
Dec	0.24	3.87	3.59
RMSE			0.408

Based on the Belgrade-Zeleno Brdo experimental data, the regression equation that represents best the relation between the D/G ratio and K is of the form:

$$D/G = 2.59 - 7.76K + 7.00K^2, \tag{1}$$

which is shown in *Fig. 2* for $0.35 \leq K \leq 0.56$. G_0 may be calculated from *Sellers* (1965) and *Robinson* (1966) using a value of 1368 W m^{-2} for the solar constant:

$$G_0 = 37.610\,(\bar{d}/d)^2\,(H \sin\varphi \sin\delta + \cos\varphi \cos\delta \sin H),$$

where $\bar{d}/d$ is the ratio of the mean to the instantaneous distance of the earth from the sun, φ is the latitude, δ is the declination angle, and H = arc cos (–tan φ tan δ) is the hour angle.

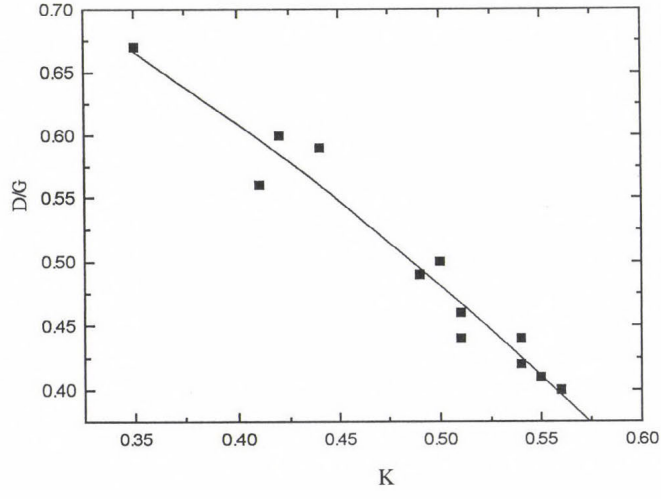

Fig. 2. D/G as a function of the 'clearness' index *K* based on Belgrade-Zeleno Brdo data (1957–1990).

The ratio of the daily diffuse to global radiation D/G was also examined by *Page* (1961) by means of data from ten locations in the belt between 40°N to 40°S. He derived the following relationship:

$$D/G = 1.00 - 1.13K. \tag{2}$$

Klein's (1977) mathematical expression for the same relation is expressed as follows:

$$D/G = 1.390 - 4.027K + 5.531K^2 - 3.108K^3, \quad \text{for } 0.4 \leq K \leq 0.5. \tag{3}$$

Using the Belgrade-Zeleno Brdo experimental data, the regression equation that represents better the relation between D/G_0 and the sunshine index I is:

$$D/G_0 = 0.208 + 0.198\,I - 0.277\,I^2, \tag{4}$$

which is shown in *Fig. 3*, for $0.25 < I < 0.64$.

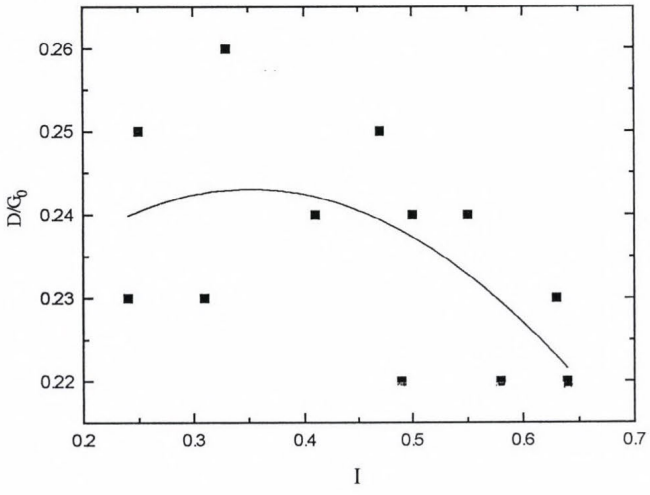

Fig. 3. D/G_0 as a function of the sunshine index I based on Belgrade-Zeleno Brdo data (1957–1990).

Hay (1965), analysing data from Canadian stations, proposed the following location-independent formulae:

$$G' = G\left\{1 + \alpha\left[\beta_0 I + \alpha_c(1 - I)\right]\right\}, \tag{5}$$

$$D'/G' = 0.9702 + 1.6688(G'/G_0) - 21.3030(G'/G_0)^2 + 51.2880(G'/G_0)^3$$
$$- 50.0810(G'/G_0)^4 + 17.5510(G'/G_0)^5 \tag{6}$$

and

$$D = D' + G\alpha\,[\beta_0 I + \alpha_c(1 - I)], \tag{7}$$

where G' and D' are the global and diffuse components of the solar radiation incident on a horizontal surface, α is the albedo (0.2) and β_0 and α_c are constants with values of 0.60 and 0.25, respectively. *Iqbal* (1979) used also data from three locations in Canada to propose the following equation:

$$D/G = 0.791 - 0.635\,I. \tag{8}$$

In order to calculate D accurately, the procedure was based on estimating D from Eqs. (1) to (8) for each month and then comparing its values with the data of Belgrade-Zeleno Brdo. The accuracy of the estimated values from the six models was tested by calculating the root mean square error (*RMSE*), which is defined as:

$$RMSE = \left\{ \frac{\left[\sum (D_{ci} - D_i)^2\right]}{12} \right\}^{\frac{1}{2}}, \tag{9}$$

where D_{ci} is the i-th calculated and D_i is the i-th measured value. Generally, lower *RMSE* records indicate that the model gives more accurate and realistic values.

The obtained results of the applied models are presented in Tables 3 and 4 with computations of *RMSE* and measured values of D for Belgrade-Zeleno Brdo and Sjenica. It can be seen that the data agree better with models (4) and (8), which include the sunshine index I, than with models (1), (2) and (3) which include the 'clearness' index K. For this reason, the values of D were calculated for Sjenica from Eq. (8) and compared with the measured values (Table 4). The calculated *RMSE,* similarly to the case of Belgrade-Zeleno Brdo indicates a good agreement between the measured and calculated values.

From the comparison of the measured values and predicted results given in Tables 3 and 4, it turns out obviously that the deviation from *Hay*'s (1965) formula is very high. Among the remaining results, the equations of *Page* (1961) show lower *RMSE* than that of *Klein*'s (1977) expression.

As there is a good agreement between the measured and calculated values of D for Belgrade-Zeleno Brdo and Sjenica stations, *Iqbal*'s (1979) equation (8) was also used to calculate the diffuse radiation at the stations where only global radiation was measured. The obtained results are presented in *Fig. 4*.

The estimation of the monthly average daily diffuse radiation D for five sites of Serbia shows that the above equation is valid for the region where the sunshine index was obtained. Also, it is very simple to use. However, *Katsoulis*'s (1991) study indicates that the diffuse solar radiation on a horizontal surface in Athens can be better estimated by using formulae proposed by *Page* (1961) and *Hay* (1965). Therefore, at moderate latitudes the local climate may have a markedly dominant effect.

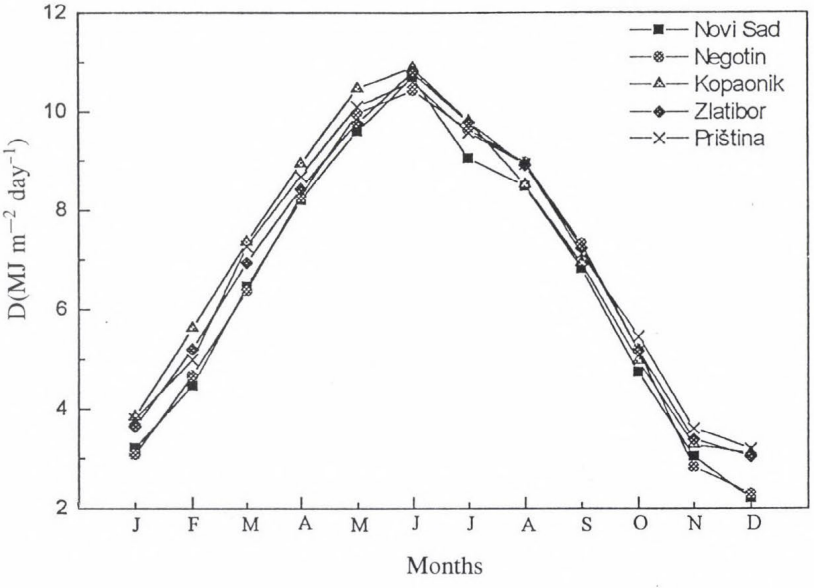

Fig. 4. Estimated annual variation of daily diffuse radiation for different stations in Serbia.

4. Conclusion

The yearly solar global and diffuse radiation in Serbia obviously depends both on the solar elevation and on the prevailing weather conditions. Based on the Belgrade-Zeleno Brdo data, the regression equations between D/G and K and D/G_0 and I lead to the conclusion that individual expressions are required for different climatic and geographic regions (see *Pasquale*, 1987).

The main conclusion of the study is that the diffuse solar radiation on horizontal surfaces in Serbia can be better estimated from formulae which include the sunshine index I, as proposed by Iqbal (1979) than from those which include the 'clearness' index K. However, the use of equations of this type is complicated by the effect of the different types of clouds as well as by significant errors in the duration of the sunshine recording.

References

Elena, A., Flocchini, G. and *Pasquale, V.*, 1981: Solar global radiation and climate at Genova, Italy. *Arch. Met. Geoph. Biol., Ser. B, 29*, 129-135.

Hay, J.E., 1965: Calculation of monthly mean solar radiation for horizontal and inclined surfaces. *Solar Energy 9*, 301-307.

Iqbal, M., 1979: A study of Canadian diffuse and total solar radiation data. *Solar Energy 22,* 81-86.

Katsoulis, B., 1991: A comparison of several diffuse solar radiation models for Greece. *Theor. Appl. Climatol. 44*, 181-186.

Katsoulis, B.D, Retalis, D.A. and *Nikolakis, D.I.*, 1991: Some solar radiation statistic for Greece. *Ann. Geophysicae 9*, 309-318.

Klein, S.A., 1977: Calculation of monthly average insolation on titled surfaces. *Solar Energy 19*, 325-329.

Lewis, G., 1987: The applicability of diffuse solar radiation model to Huntsville, Alabama. *Solar Energy 38*, 55-57.

Page, J.K., 1961: The estimation of monthly mean values of daily total short-wave radiation on vertical and inclined surfaces, from sunshine records for latitudes 40°N to 40°S. *Proc. of UN Cont. on New Sources of Energy*, Rome, Italy.

Pasquale, V., 1987: Solar irradiance in NW Italy. *Theor. Appl. Climatol. 38*, 85-92.

Robinson, N., 1966: *Solar Radiation*. Elsevier, New York.

Santamouris, M. and *Katsoulis, B.*, 1989: Solar radiation over the northwest part of Greece. *Solar and Wind Technology 6*, No. 1, 79-84.

Sellers, W.D., 1965: *Physical Climatology*. University of Chicago Press, Chicago.

BOOK REVIEWS

Hervé Le Treut (ed.): **Climate Sensitivity to Radiative Perturbations. Physical Mechanisms and Their Validation.** Srpinger-Verlag 1996. ISBN 3-540-60434-0. NATO Advanced Science Institutes Series Vol. 34. pp. 330, price 378 DEM.

This book gathers many of the papers, both invited and contributed, which were presented during the NATO Advanced Research Workshop on *'Climate Sensitivity to Radiative Perturbations'*, held in Paris, July 1994. A workshop dedicated to the FANGIO (Feedback Analysis of General Circulation Models for Intercomparison and Observation) programme was embedded within the NATO workshop, and some of the papers presented in the book correspond to this programme.

Section 1 contains contributions which are not dedicated to the study of one model but address more general or methodological issues. Many of the questions raised in this section receive answers, directly or indirectly, within the papers of Section 2 and 3 which concern individual models. In Section 1 presented are details of investigations on the Atmospheric Model Intercomparison Project including results concerning radiative forcing calculated by means of 25 different models, absorption of solar radiation by clouds, evaluation of variability of tropical convection in GCMs by using geostationary satellite data, impact of volcanic eruption on global temperature, stochastic models to represent the temporal variability of global average radiation budget and temperature.

Section 2: 'Cloud and water vapour feedbacks in atmospheric models' presents many details of results obtained from research on warm pool heat budget by different versions of the ECHAM model developed at the Max Planck Institute, Hamburg; GCM implications for mechanism determining cloud and water vapour feedbacks, comparison of convection parameterisations in an atmospheric GCM, sensitivity of the simulated climate to parameterisation of cloud optical properties in GCM, the role of cloud-radiative interactions in the sensitivity of the ECMWF model, water vapor and cloud feedback in Atmospheric General Circulation Models, cloud feedbacks in the UKMO unified model etc.

Section 3: 'Feedbacks in coupled ocean-atmosphere models' contains papers concerning the climate sensitivity and cloud-albedo feedback in a global coupled ocean-atmosphere GCM, cloud effects on the ocean surface energy budget, feedback processes in the GFDL (Geophysical Fluid Dynamics Laboratory) R 30–14 level GCM, aerosol and greenhouse gases forcing, analysis of the monsoon response to radiative perturbations in GCM simu-

lations, large scale atmosphere-ocean interaction and climate, a 65–70 year oscillation in observed surface temperatures.

Altogether 43 researchers and lecturers from 12 countries and at least 20 institutions took part in the meeting.

G. Koppány

C.D. Schönwiese: **Klimaänderungen. Daten, Analysen, Prognosen.** Springer-Verlag, 1995, ISBN 3-540-59096-X. pp. 226, 58 figures, several colour photos, 16 tables.

The author has been a professor of meteorology at the University of Frankfurt/Main since 1981 and director of the Environment Research Centre at the same University since 1994. He is well known as an excellent expert in the field of climate variation and a skilled investigator concerning global change. He is a scientific adviser at WMO, as well.

This book comprises the most important elements of climatology including the term or definition of climate, the time scales of the atmospheric phenomena, the survey of the climate system (Chapter 1), the sources of climate data including paleoclimatic information, e.g. historical data, glacier expansions, pollen analyses etc. (Chapter 2). Statistical methods most frequently applied in climatology (Chapter 3), a very good summary of methods and results of paleoclimatology (Chapter 4), the natural factors causing climate changes (Chapter 5), some features of climate models (Chapter 6), the consequences of human activity in global change (Chapter 7), and the possible future of climate (Chapter 8). The simple survey of subjects discussed in individual chapters may convince the reader that is this book one can find elementary knowledge on climatology as well as up-to-date information on the past climate of the earth including some methods of paleoclimatology, the recent assessments on the future of our climate making use of the newest climate models. The didactics of the book's construction is so good that the reader is attracted to read over all the chapters one after the other from the first to the last one. In addition to the newest knowledge, this book presents several color photos, one of them made by a satellite.

Finally the author attaches the symbols and abbreviations used most frequently in the book as well as the list of additional recent works concerning the relevant topic. About 130 books and papers are cited.

G. Koppány

ATMOSPHERIC ENVIRONMENT

an international journal

To promote the distribution of Atmospheric Environment *Időjárás* publishes regularly the *contents* of this important journal. For further information the interested reader is asked to contact *Prof. P. Brimblecombe,* School for Environmental Sciences, University of East Anglia, Norwich NR4 7TJ, U.K. E-mail: atmos_env@uea.ac.uk

Volume 31 Number 1 1997

Volume 31 Number 2 1997

Volume 31 Number 3 1997

The Dutch Aerosol Project (1992–1994)
Plus Regular Papers

M.W. Gallagher, K.M. Beswick, J. Duyzer, H. Westrate, T.W. Choularton and *P. Hummelshøj:* Measurements of aerosol fluxes to Speulder Forest using a micrometeorological technique, 359-373.

A.T. Vermeulen, G.P. Wyers, F.G. Römer, N.F.M. Van Leeuwen, G.P.J. Draaijers and *J.W. Erisman:* Fog deposition on a coniferous forest in The Netherlands, 375-386.

G.P.J. Draaijers, J.W. Erisman, N.F.M. Van Leeuwen, F.G. Römer, B.H. Te Winkel, A.C. Veltkamp, A.T. Vermeulen and *G.P. Wyers:* The impact of canopy exchange on differences observed between atmospheric deposition and throughfall fluxes, 387-397.

W. Ruijgrok, H. Tieben and *P. Eisinga:* The dry deposition of particles to a forest canopy: a comparison of model and experimental results, 399-415.

Regular Papers

M.J. Ten Harkel: The effects of particle-size distribution and chloride depletion of sea-salt aerosols on estimating atmospheric deposition at a coastal site, 417-427.

M. Bennett and *G.C. Hunter:* Some comparisons of Lidar estimates of peak ground-level concentrations with the predictions of UK-ADMS, 429-439.

S. Parat, A. Perdrix, H. Fricker-Hidalgo, I. Saude, R. Grillot and *P. Baconnier:* Multivariate analysis comparing microbial air content of an air-conditioned building and a naturally ventilated building over one year, 441-449.

E. Weingartner, C. Keller, W.A. Stahel, H. Burtscher and *U. Baltensperger:* Aerosol emission in a road tunnel, 451-462.

C.-S. Chen and *C.-Y. Lin:* A numerical study of airflow over Taiwan Island, 463-473.

G.R. Carmichael, A. Sandu and *F.A. Potra:* Sensitivity analysis for atmospheric chemistry models via automatic differentiation, 475-489.

Z. Cvetnić and *S. Pepeljnjak:* Distribution and mycotoxin-producing ability of some fungal isolates from the air, 491-495.

B.C. Faust, K. Powell, C.J. Rao and *C. Anastasio:* Aqueous-phase photolysis of biacetyl (an α-dicarbonyl compound): a sink for biacetyl, and a source of acetic acid, peroxyacetic acid, hydrogen peroxide, and the highly oxidizing acetylperoxyl radical in aqueous aerosols, fogs, and clouds, 497-509.

Volume 31 Number 4 1997

M. Piringer, K. Baumann, H. Rötzer, J. Riesing and *K. Nodop:* Results on perfluorocarbon background concentrations in Austria, 515-527.

S.-O. Baek, Y.-S. Kim and *R. Perry:* Indoor air quality in homes, offices and restaurants in Korean urban areas—indoor/outdoor relationships, 529-544.

A. Virkkula: Performance of a differential optical absorption spectrometer for surface O_3 measurements in the Finnish Arctic, 545-555.

D. Brocco, R. Fratarcangeli, L. Lepore, M. Petricca and *I. Ventrone:* Determination of aromatic hydrocarbons in urban air of Rome, 557-566.

M.H. Hermanson, C.L. Monosmith and *M.T. Donnelly-Kelleher:* Seasonal and spatial trends of certain chlorobenzene isomers in the Michigan atmosphere, 567-573.

M. Gonzalez: Analysis of the effect of microscale turbulence on atmospheric chemical reactions by means of the p.d.f. approach, 575-586.

M. Z. Jacobson: Development and application of a new air pollution modeling system—Part III. Aerosol-phase simulations, 587-608.

T. Castro, L.G. Ruiz-Suárez, J.C. Ruiz-Suárez, M.J. Molina and *M. Montero:* Sensitivity analysis of a UV radiation transfer model and experimental photolysis rates of NO_2 in the atmosphere of Mexico City, 609-620.

Volume 31 Number 5 1997

Short Communications

Volume 31 Number 6 1997

Volume 31 Number 7 1997

NOTES TO CONTRIBUTORS

The purpose of *Időjárás* is to publish papers in the field of theoretical and applied meteorology. These may be reports on new results of scientific investigations, critical review articles summarizing current problems in certain subject, or shorter contributions dealing with a specific question. Authors may be of any nationality but papers are published only in English.

Papers will be subjected to constructive criticism by unidentified referees.

* * *

The manuscript should meet the following formal requirements:

Title should contain the title of the paper, the names(s) of the author(s) with indication of the name and address of employment.

The title should be followed by an *abstract* containing the aim, method and conclusions of the scientific investigation. After the abstract, the *key-words* of the content of the paper must be given.

Three copies of the manuscript, typed with double space, should be sent to the Editor-in-Chief: *P.O. Box 39, H-1675 Budapest,* Hungary.

References: The text citation should contain the name(s) of the author(s) in Italic letter or underlined and the year of publication. In case of one author: *Miller* (1989), or if the name of the author cannot be fitted into the text: *(Miller,* 1989); in the case of two authors: *Gamov* and *Cleveland* (1973); if there are more than two authors: *Smith et al.* (1990). When referring to several papers published in the same year by the same author, the year of publication should be followed by letters a,b etc. At the end of the paper the list of references should be arranged alphabetically. For an article: the name(s) of author(s) in Italics or underlined, year, title of article, name of journal, volume number (the latter two in Italics or underlined) and pages. E.g. *Nathan, K. K.,* 1986: A note on the relationship between photosynthetically active radiation and cloud amount. *Időjárás 90,* 10-13. For a book: the name(s) of author(s), year, title of the book (all in Italics or underlined with except of the year), publisher and place of publication. E.g. *Junge, C. E.,* 1963: *Air Chemistry and Radioactivity.* Academic Press, New York and London.

Figures should be prepared entirely in black India ink upon transparent paper or copied by a good quality copier. A series of figures should be attached to each copy of the manuscript. The legends of figures should be given on a separate sheet. Photographs of good quality may be provided in black and white.

Tables should be marked by Arabic numbers and provided on separate sheets together with relevant captions. In one table the column number is maximum 13 if possible. One column should not contain more than five characters.

Mathematical formulas and *symbols:* non-Latin letters and hand-written marks should be explained by making marginal notes in pencil.

The final text should be submitted both in manuscript form and on *diskette.* Use standard 3.5" or 5.25" DOS formatted diskettes for this purpose. The following word processors are supported: WordPerfect 5.1, WordPerfect for Windows 5.1, Microsoft Word 5.5, Microsoft Word 6.0. In all other cases the preferred text format is ASCII.

* * *

Authors receive 30 *reprints* free of charge. Additional reprints may be ordered at the authors' expense when sending back the proofs to the Editorial Office.

Published by the Hungarian Meteorological Service

Budapest, Hungary

INDEX: 26 361

HU ISSN 0324-6329